

Searching for a Heavy Higgs boson in a Higgs-portal B-L Model

Shankha Banerjee,^{1,*} Manimala Mitra,^{2,†} and Michael Spannowsky^{3,‡}

¹*Regional Centre for Accelerator-based Particle Physics,*

Harish-Chandra Research Institute,

Chhatnag Road, Jhusi, Allahabad 211019, India.

²*Indian Institute of Science Education and Research Mohali,*

Knowledge city, Sector 81, SAS Nagar, Manauli PO 140306.

³*Institute for Particle Physics Phenomenology,*

Durham University, Durham DH1 3LE, United Kingdom.

Abstract

We study the discovery prospects of a heavy neutral scalar arising from a $U(1)_{B-L}$ extension of the Standard Model (SM) during the Large Hadron Collider's high luminosity runs (HL-LHC). This heavy neutral scalar mixes with the SM Higgs boson through a Higgs portal and interacts with the SM particles with an interaction strength proportional to the sine of the mixing angle. The mixing between the two Higgs bosons is constrained by direct and indirect measurements. We choose an experimentally viable mixing angle and explore in detail the ZZ and WW decay modes of the heavy Higgs boson. For the ZZ case, we focus on the cleanest 4ℓ and $2\ell 2j$ final states and find that a heavy Higgs boson of mass smaller than 500 GeV can be discovered at the HL-LHC. For the WW decay mode, we analyze the $\ell jj \cancel{E}_T$ signature. We implement novel background reduction techniques in order to tackle the huge background by performing both cut-based and multivariate analyses. However, large backgrounds render this channel challenging. We briefly discuss the discovery prospects of the heavy Z' -boson arising in this model.

PACS numbers: 12.60.-i, 12.60.Cn, 12.60.Fr

Keywords: B-L model, Singlet Extension, HL-LHC

* shankha@hri.res.in

† manimala@iisermohali.ac.in

‡ michael.spannowsky@durham.ac.uk

I. INTRODUCTION

The CMS and ATLAS collaborations at the Large Hadron Collider (LHC) have successfully discovered a new resonance [1, 2] with a mass of 125 GeV [3], which has properties consistent with the Higgs boson predicted by the Standard Model (SM). The signal strengths of this boson in its various final states are in good agreement with the SM expectations at 1σ . The nominal variations in certain production and decay modes could be due to some physics beyond the standard model (BSM) or could simply be due to insufficient statistics.

It is well known that the SM cannot be the final theory of nature. The successful explanation of the hierarchy problem requires some new physics (NP) near the TeV scale. In addition, the observation of small neutrino masses and their very particular mixing indicates the presence of physics beyond the standard model (BSM). There are a few well motivated theories, such as supersymmetric extensions of the SM or theories with extra spatial dimensions, that cure the aforementioned limitations of the SM. However, neither ATLAS nor CMS have yet conclusively discovered any particle that serves as proof for BSM physics. Now, with the discovery of the Higgs boson, effects of new physics can be searched for in its coupling measurements [4–37].

In this paper, we consider the simplest manifestation of a BSM extension through an extra singlet scalar. As a first step, we would like to see how the addition of just an additional neutral Higgs boson fares with the discovery prospects at the high-luminosity run at LHC (HL-LHC) with a final integrated luminosity of 3000 fb^{-1} .

The presence of a heavy Higgs-like neutral scalar is innate in various models, such as, the minimal supersymmetric standard model (MSSM), two Higgs doublet models (2HDMs), models with extra spatial dimensions, etc. However, the simplest among these models is the SM augmented with a gauge singlet. This can originate very naturally from a $U(1)_{B-L}$ model with an extra $U(1)$ local gauge symmetry [38], where B and L represents the baryon number and lepton number respectively. In particular, we focus on a TeV scale $B-L$ model, that can further be embedded in a TeV scale Left-Right symmetric model [39–43]. The $B-L$ symmetry group is a part of a Grand Unified Theory (GUT) as described by a $SO(10)$ group [44]. Besides, the $B-L$ symmetry breaking scale is related to the masses of the heavy right-handed Majorana neutrinos, which participate in the celebrated *seesaw* mechanism [45–48] and generate the light neutrino masses.

Another important theoretical motivation of this model is that the right handed neu-

trinos, that are an essential ingredient of this model participate in generating the baryon asymmetry of the universe via leptogenesis [49]. Hence, the $B - L$ breaking scale is strongly linked to leptogenesis via sphaleron interactions that preserve $B - L$. It is important to note that in the $U(1)_{B-L}$ model, the symmetry breaking can take place at scales much lower than that of any GUT scale, e.g. the electroweak (EW) scale or TeV scale. Because the $B + L$ symmetry is broken due to sphaleron interactions, baryogenesis or leptogenesis cannot occur above the $B - L$ breaking scale. Hence, the $B - L$ breaking around the TeV scale naturally implies TeV scale baryogenesis.

The presence of heavy neutrinos, a TeV scale extra neutral gauge boson and an additional heavy neutral Higgs, makes the model phenomenologically rich, testable at the LHC as well as future e^+e^- colliders [50–63]. The Majorana nature of the heavy neutrinos can be probed for example through same-sign dileptonic signatures at the LHC [64]. On the other hand, the extra gauge boson Z' in this model interacts with SM leptons and quarks. Non-observation of an excess in dilepton and di-jet signatures by ATLAS and CMS have placed stringent constraints on the Z' mass [65–70].

In this work, we examine in detail the discovery prospects of the second Higgs at the HL-LHC for a TeV scale $U(1)_{B-L}$ model. The vacuum expectation value (vev) of the gauge singlet Higgs breaks the $U(1)_{B-L}$ symmetry and generates the masses of the right handed neutrinos. We consider the $B - L$ breaking scale to be of the order of a few TeVs, for which the right handed neutrino masses can naturally be in the TeV range. The physical second Higgs state mixes with the SM Higgs boson with a mixing angle θ , constrained by electroweak precision measurements from LEP [71–73], as well as from Higgs coupling measurements at LHC [74, 75]. The second Higgs is dominantly produced by gluon fusion with subsequent decay into heavy particles. The largest branching ratios are into W , Z and Higgs bosons. We discuss in detail the different channels through which the second Higgs state can be probed at the HL-LHC.

Note that there are other possible $B - L$ extensions of the SM, that have been studied in Refs. [76], Refs. [77] and Refs. [78]. In Refs. [76], the $B - L$ gauge boson Z' acquires mass through the Stueckelberg mechanism [79, 80]. In this case, the $B - L$ symmetry is unbroken, even after Z' acquires mass. Hence, the neutrinos in this model are necessarily of Dirac nature. To generate the mass of Z' via Stueckelberg mechanism, the presence of an axionic scalar is required. In addition to the $U(1)_{B-L}$, an additional $U(1)_X$ symmetry is imposed, that brings down the scale of the Z' around TeV. As a second option [78],

the $B - L$ symmetry is broken spontaneously by an SM gauge singlet Higgs field and as a consequence the Z' acquires mass. However, due to non-trivial $B - L$ charge assignment of the gauge singlet Higgs, this scenario does not contain any Majorana mass term of the heavy right handed neutrinos. The light neutrinos in this model are again necessarily of Dirac nature. The collider signatures of these models are very different compared to the $B - L$ extension where the light and heavy neutrinos are of Majorana nature.

The paper is organised as follows: in section II, we review the basics of the $U(1)_{B-L}$ model. We discuss the constraints on the heavy neutrino sector and the limits on Z' in section III. Following this, in section IV, we outline the different constraints on the mixing angle between the SM-like Higgs and the second Higgs state. We study in detail the collider signatures of the heavy Higgs in section V. We briefly discuss non-standard production of the heavy Higgs in section VI. Decay of the heavy Higgs to a pair of heavy neutrinos is discussed in section VII. Eventually we offer conclusions in section VIII.

II. BRIEF REVIEW OF THE $U(1)_{B-L}$ MODEL

The $U(1)_{B-L}$ model is one of the simplest extensions of the SM [44, 81–85]. In addition to the symmetry group of the SM, it has an additional $U(1)$ gauge symmetry, that is identified as $B - L$ symmetry. The full group structure of this model is therefore

$$SU(3)_C \times SU(2)_L \times U(1)_Y \times U(1)_{B-L}, \quad (1)$$

where $U(1)_{B-L}$ represents the additional gauge symmetry. The Lagrangian of this model is as follows:

$$\mathcal{L} = \mathcal{L}_s + \mathcal{L}_{YM} + \mathcal{L}_f + \mathcal{L}_Y, \quad (2)$$

where $\mathcal{L}_s, \mathcal{L}_{YM}, \mathcal{L}_f$ and \mathcal{L}_Y are the scalar, Yang-Mills, fermion and Yukawa terms respectively. The different terms in the Lagrangian are explained in detail in Refs. [51, 52, 57].

The Yang-Mills Lagrangian can be expressed as

$$\mathcal{L}_{YM} = -\frac{1}{4}G_{\mu\nu}^a G^{a,\mu\nu} - \frac{1}{4}W_{\mu\nu}^b W^{b,\mu\nu} - \frac{1}{4}F_{\mu\nu} F^{\mu\nu} - \frac{1}{4}F'_{\mu\nu} F'^{\mu\nu}, \quad (3)$$

where the first three terms represent the kinetic terms of the $SU(3)_C, SU(2)_L$ and $U(1)_Y$ gauge groups respectively. a, b are the colour and $SU(2)$ indices respectively. The fourth term is the kinetic term for the $U(1)_{B-L}$ gauge group and is represented by

$$F'_{\mu\nu} = \partial_\mu B'_\nu - \partial_\nu B'_\mu, \quad (4)$$

where B' is the $U(1)_{B-L}$ field strength.

In addition to the standard particle contents of SM, the fermion sector of this model has three right-handed neutrinos N_R , that are singlets under SM gauge group. This is required for anomaly cancellation and these right handed neutrinos generate Majorana masses of the light neutrinos through the *seesaw* mechanism, as discussed in section III. Analogous to the SM, the covariant derivative for this model is defined as

$$D_\mu = \partial_\mu + ig_s t^a G_\mu^a + ig T^b W_\mu^b + ig_1 Y B_\mu + ig' Y_{B-L} B'_\mu, \quad (5)$$

where g_s, g, g_1 and g' are the $SU(3)_C, SU(2)_L, U(1)_Y$ and $U(1)_{B-L}$ couplings with t^a, T^b, Y and Y_{B-L} being their respective group generators. In the present study, we explicitly assume that there is no direct mixing between the two $U(1)$ fields B and B' . This corresponds to the minimal version of the $B - L$ model. The fermion sector of the Lagrangian is expressed by

$$\begin{aligned} \mathcal{L}_f = \sum_{i=1,2,3} & (i \overline{(Q_L)_i} \gamma^\mu D_\mu (Q_L)_i + i \overline{(u_R)_i} \gamma^\mu D_\mu (u_R)_i + i \overline{(d_R)_i} \gamma^\mu D_\mu (d_R)_i \\ & + i \overline{(L_L)_i} \gamma^\mu D_\mu (L_L)_i + i \overline{(e_R)_i} \gamma^\mu D_\mu (e_R)_i + i \overline{(N_R)_i} \gamma^\mu D_\mu (N_R)_i), \end{aligned} \quad (6)$$

where the electromagnetic charges on the fields are the same as the SM ones and the $B - L$ charges are $Y_{B-L}^{quarks} = \frac{1}{3}$ and $Y_{B-L}^{leptons} = -1$.

In order to break the $B - L$ gauge symmetry and to generate the mass of the additional Z' boson corresponding to this extra gauge symmetry, one needs to introduce an extra complex Higgs field χ . The field χ is a singlet under the SM gauge group with non-zero $B - L$ charge $Y_{B-L}^\chi = +2$. The $B - L$ symmetry is broken spontaneously by the *vev* of the Higgs field χ . The SM Higgs field is neutral under the $B - L$ gauge group, hence it has $Y_{B-L}^H = 0$. This particular choice preserves gauge invariance.

The most general and renormalisable scalar Lagrangian of this model can be expressed as

$$\mathcal{L}_s = (D^\mu H)^\dagger D_\mu H + (D^\mu \chi)^\dagger (D_\mu \chi) - V(\chi, H), \quad (7)$$

where the scalar potential $V(\chi, H)$ has the following form,

$$V(\chi, H) = M_H^2 H^\dagger H + m_\chi^2 |\chi|^2 + \lambda_1 (H^\dagger H)^2 + \lambda_2 |\chi|^4 + \lambda_3 (H^\dagger H) |\chi|^2. \quad (8)$$

To complete the discussion on the Lagrangian, we write down the Yukawa term, which

in addition to the SM terms has interactions involving the right-handed neutrinos N_R ,

$$\begin{aligned} \mathcal{L}_Y = & -y_{ij}^d \overline{(Q_L)_i} (d_R)_j H - y_{ij}^u \overline{(Q_L)_i} (u_R)_j \tilde{H} - y_{ij}^e \overline{(L_L)_i} (e_R)_j H \\ & - y_{ij}^\nu \overline{(L_L)_i} (N_R)_j \tilde{H} - y_{ij}^M \overline{(N_R)_i^c} (N_R)_j \chi + h.c., \end{aligned} \quad (9)$$

where $\tilde{H} = i\sigma^2 H^*$ and i, j runs from 1-3. The vev of the χ field breaks the $B - L$ symmetry and generates the Majorana masses of the right handed neutrinos N_R where $M_{N_R} = y^M v'$. On the other hand, the Dirac masses for the light neutrinos are governed by the Yukawa couplings y^ν 's.

Next, we turn our attention to spontaneous electroweak symmetry breaking (SSB) in this model. Further details are discussed in Ref. [57]. In order for the potential to be bounded from below, the couplings $\lambda_{1,2,3}$ should be related as

$$\begin{aligned} 4\lambda_1\lambda_2 - \lambda_3^2 &> 0, \\ \lambda_{1,2} &> 0. \end{aligned} \quad (10)$$

In order to minimise the potential, one requires the above two conditions to hold.

We denote the $vevs$ of H and χ by v and v' respectively. On minimising the potential $V(\chi, H)$ with respect to both $vevs$, one obtains [51, 52, 57],

$$v^2 = \frac{4\lambda_2 M_H^2 - 2\lambda_3 M_\chi^2}{\lambda_3^2 - 4\lambda_1\lambda_2}, \quad v'^2 = \frac{4\lambda_1 M_\chi^2 - 2\lambda_3 M_H^2}{\lambda_3^2 - 4\lambda_1\lambda_2}. \quad (11)$$

Since the $B - L$ breaking scale is higher than the electroweak symmetry breaking (EWSB) scale, we have $v' > v$.

χ mixes with H due to the λ_3 -term as shown in Eq. 8. The mass matrix between the two Higgs bosons in the basis (H, χ) is given by

$$\mathcal{M}(H, \chi) = 2 \begin{pmatrix} \lambda_1^2 v^2 & \lambda_3 v v' / 2 \\ \lambda_3 v v' / 2 & \lambda_2 v'^2 \end{pmatrix}. \quad (12)$$

Next, we define the mass eigenstates as (H_1, H_2) which are related to the (H, χ) basis by

$$\begin{pmatrix} H_1 \\ H_2 \end{pmatrix} = \begin{pmatrix} \cos \theta & -\sin \theta \\ \sin \theta & \cos \theta \end{pmatrix} \begin{pmatrix} H \\ \chi \end{pmatrix}, \quad (13)$$

where the mixing angle θ ($-\frac{\pi}{2} < \theta < \frac{\pi}{2}$) satisfies

$$\tan 2\theta = \frac{\lambda_3 v' v}{(\lambda_2 v'^2 - \lambda_1 v^2)}. \quad (14)$$

The masses of the physical Higgs bosons, H_1 and H_2 are

$$\begin{aligned} M_{H_1}^2 &= \lambda_1 v^2 + \lambda_2 v'^2 - \sqrt{(\lambda_1 v^2 - \lambda_2 v'^2)^2 + \lambda_3^2 v'^2 v^2}, \\ M_{H_2}^2 &= \lambda_1 v^2 + \lambda_2 v'^2 + \sqrt{(\lambda_1 v^2 - \lambda_2 v'^2)^2 + \lambda_3^2 v'^2 v^2}. \end{aligned} \quad (15)$$

After imposing SSB in \mathcal{L}_s , one obtains the mass spectrum of the gauge bosons

$$\begin{aligned} M_\gamma &= 0, \\ M_{W^\pm} &= \frac{1}{2}vg, \\ M_Z &= \frac{v}{2}\sqrt{g^2 + g_1^2}, \\ M_{Z'} &= 2v'g'. \end{aligned} \quad (16)$$

Note that, among the two Higgs masses, one chooses $m_{H_1}^2 < m_{H_2}^2$, *i.e.*, H_1 is chosen to be the lightest state. In our subsequent discussion we will consider the case, where H_1 is SM-like with a mass around 125 GeV. The other Higgs state, H_2 is heavy and we allow its mass to vary in the range 250-900 GeV for our phenomenological studies. The interactions of H_1 and H_2 with the fermions and gauge bosons are expressed in terms of the mixing parameter θ in the following manner

$$\begin{aligned} H_1 f \bar{f} &: -\frac{eM_f \cos \theta}{2M_W}, & H_2 f \bar{f} &: -\frac{eM_f \sin \theta}{2M_W}, \\ H_1 W^+ W^- &: \frac{M_W e \cos \theta}{s_w}, & H_2 W^+ W^- &: \frac{M_W e \sin \theta}{s_w}, \\ H_1 Z Z &: \frac{M_W e \cos \theta}{c_w^2 s_w}, & H_2 Z Z &: \frac{M_W e \sin \theta}{c_w^2 s_w}, \\ H_1 Z' Z' &: -8 \sin \theta g'^2 v', & H_2 Z' Z' &: -8 \cos \theta g'^2 v'. \end{aligned} \quad (17)$$

The scalar self-interactions are given by

$$\begin{aligned} H_1 H_1 H_1 &: -3\frac{1}{e}(4 \cos^3 \theta \sin \theta_w M_W \lambda_1 - 2 \sin^3 \theta e \lambda_2 v' - \\ &\quad \cos^2 \theta \sin \theta e \lambda_3 v' + 2 \sin \theta_w \sin^2 \theta \cos \theta M_W \lambda_3), \\ H_2 H_1 H_1 &: -\frac{1}{e}(12 \cos^2 \theta \sin \theta_w \sin \theta M_W \lambda_1 + 6 \sin^2 \theta \cos \theta e \lambda_2 v' + \\ &\quad (1 - 3 \sin^2 \theta) \cos \theta e \lambda_3 v' - 2(2 - 3 \sin^2 \theta) \sin \theta_w \sin \theta M_W \lambda_3). \end{aligned} \quad (18)$$

In the above expressions, f denotes the SM fermions. We refer the readers to Refs. [51, 52, 57] for a detailed description of the other interaction terms, arising from this model. Since, there are no extra coloured or electromagnetically charged states in this model that can alter the loop functions, we calculate the effective vertices $ggH_{1,2}$, $\gamma\gamma H_{1,2}$, $Z\gamma H_{1,2}$ and $Z'\gamma H_{1,2}$ following the standard loop functions relevant for the SM (see [86] and references therein).

III. CONSTRAINTS ON HEAVY NEUTRINOS AND Z'

Before proceeding to discuss the phenomenological aspects of the heavy Higgs, we briefly discuss the constraints and limits on the various parameters arising from the heavy neutrinos N_R and Z' .

A. Constraints on Heavy Neutrinos

As we discussed in the previous section, the model consists of three right-handed neutrinos N_R , required for anomaly cancellation in the theory. The low-scale breaking of the $B - L$ gauge symmetry implies the right handed neutrinos to be of the order of a few hundred GeVs to a few TeVs. In this work, we consider the heavy right handed neutrinos of TeV scale, that naturally emerge from low scale $B - L$ breaking, without any unnatural tuning of the Yukawas. This scale will be accessible in the coming runs of the LHC and possibly also at future lepton and hadron collider experiments. The right handed neutrinos generate the masses for the light neutrinos via the *seesaw* mechanism

$$\mathcal{M}_\nu = -M_D^T M_R^{-1} M_D. \quad (19)$$

In the above, M_D is the Dirac mass matrix of light neutrinos, whereas M_R is the Majorana mass matrix of the heavy neutrinos. By demanding $M_R \sim \text{TeV}$ and $\mathcal{M}_\nu \sim \text{eV}$, one is able to constrain the active-sterile neutrino mixing $M_D/M_R \sim 10^{-6}$. In addition to the constraints from light neutrino masses, the active-sterile mixing can also be constrained from other experimental searches, e.g. the neutrino-less double beta decay ($0\nu 2\beta$), β -decay, peak searches and kink searches [50, 63, 87]. The heavy Majorana neutrino, that mix with the active light neutrino ν with a mixing angle θ_ν , participate in the $0\nu 2\beta$ -decay, where the amplitude is expressed as

$$\mathcal{A}_N \sim G_F^2 \frac{\theta_\nu^2}{M_R}. \quad (20)$$

The non-observation of any positive signal in this lepton number violating process constrains the active-sterile mixing to $\theta_\nu^2 < 10^{-5}$, for a heavy neutrino mass $M_R \sim 500 \text{ GeV}$ [88]. A complete discussion on the different bounds on the active-sterile neutrino mixing can be found in [87, 89]. In addition, the collider signatures of the heavy neutrinos at LHC has been discussed in details in Ref. [54]. A detailed discussion of the like sign dilepton signature from right handed neutrino decay has been studied in Ref. [54].

B. Limits on Z'

The $B - L$ model has an additional gauge boson Z' of mass $M_{Z'} = 2v'g'_1$. Z' interacts with the leptons, quarks, heavy neutrinos and light neutrinos with interaction strengths proportional to the $B - L$ gauge coupling g' . The Z' boson can in principle be detected by observing di-leptonic and di-jet signals at colliders. The presence of a sequential SM-like (SSM) Z' gauge boson has been severely constrained by direct searches at colliders, as well as by indirect searches. The ratio of Z' mass to its coupling is constrained from indirect searches to be around [52, 77, 90, 91]

$$\frac{M_{Z'}}{g'} \geq 6.9 \text{ TeV}. \quad (21)$$

Several studies have been carried out by ATLAS and CMS in di-leptonic and di-jet channels to search for this elusive heavy gauge boson [65–70]. The Z' can decay to a boosted $t\bar{t}$ pair which provides sensitivity in semi-leptonic or fully hadronic top decays [69, 92]. The cross-section times branching ratio ($\sigma \times B$) has been constrained to be less than 1–2 pb [69] for a Z' with a width to mass ratio between $\Gamma_{Z'}/M_{Z'} = 1\%$ and $\Gamma_{Z'}/M_{Z'} = 10\%$. Note that, here and in Table. I, we quote the most conservative limits of the cross-sections, where for other different masses the cross-sections are even more stringent. The recent combined analysis by CMS for the di-electron and di-muon mass spectra has further constrained the ratio (R) of cross-section times branching ratio of a narrow resonance [67]. In addition, the di-leptonic search by ATLAS has also constrained the sequential Z' [66]. The other searches correspond to

1. The search for a di-jet resonance by CMS [68] that constrains $\sigma \times B \times A < 0.2 - 0.3$ pb (A being the acceptance for the kinematic requirements) and $M_{Z'_{SSM}} < 1.70$ TeV
2. ATLAS search for $\tau^+\tau^-$ pair [70]
3. CMS search for heavy resonance into $b\bar{b}$ pairs that bounds $M_{Z'_{SSM}}$ [65].

In addition, we also show the limits applicable for a $B - L$ model by comparing the limits from the 8 TeV run of the ATLAS di-lepton search [66], in Fig. 1. We consider few benchmark values for the free parameter g' and also for the mass of the heavy neutrino. Note that the production cross-sections of Z' in the $B - L$ model have been computed at leading order (LO). The bounds on $M_{Z'}$ from this model are summarised in Table II.

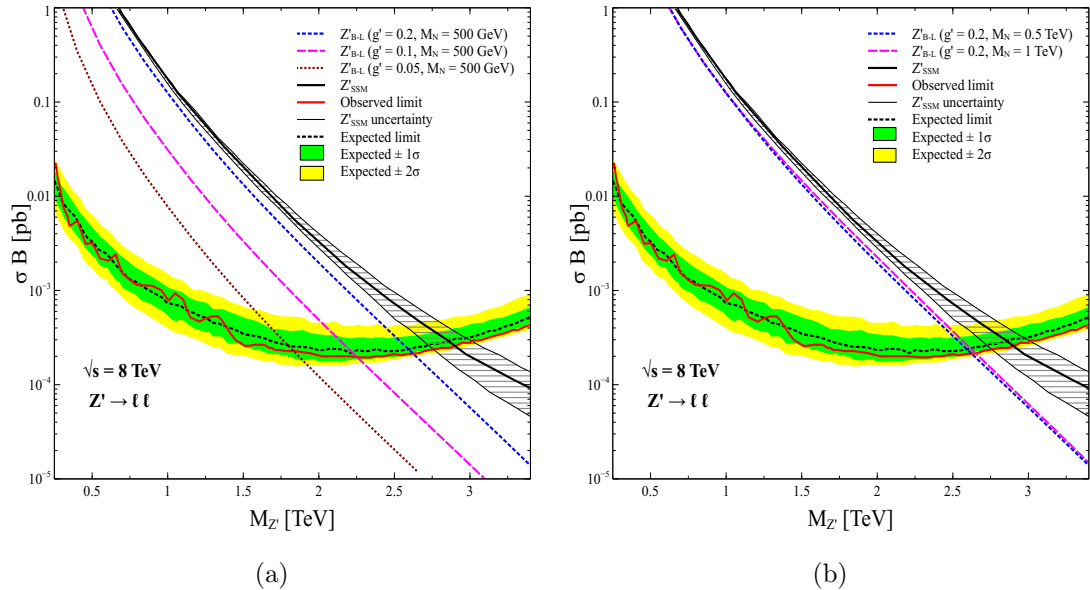


FIG. 1. The comparison between the limits from ATLAS di-lepton search [66] with the $B - L$ predictions with (a) $M_N = 500$ GeV and $g' = 0.05$ (brown fine dotted), $g' = 0.1$ (magenta dashed) and $g' = 0.2$ (blue dotted) and (b) $g' = 0.2$ and $M_N = 500$ GeV (blue dotted) and $M_N = 1$ TeV (magenta dashed).

In Fig. 1a, we find that by varying the coupling parameter g' , the bound on $M_{Z'}$ changes considerably by a few 100 GeV, whereas in Fig. 1b, we find that by varying the masses of the heavy neutrinos, the bounds shift by $\mathcal{O}(10)$ GeV¹. Finally, we give an estimate of how the signal fares with respect to the SM backgrounds by studying the di-lepton final state using a basic set of trigger cuts on the transverse momentum (p_T), pseudo-rapidity (η) and isolation in the pseudo-rapidity-azimuthal angle plane (ΔR), i.e. $p_{T,\ell} > 10$ GeV, $|\eta_\ell| < 2.5$ and $\Delta R_{\ell\ell} > 0.2$. For the 14 TeV run, the benchmark $M_{Z'} = 3$ TeV and $g' = 0.2$ yields the LO cross-section to be around 1.4 fb. Whereas, for the background the LO cross-section is around 1900 pb, several orders of magnitude larger than the signal cross-section. However, by imposing a simple invariant mass cut on the dilepton system, $2900 \text{ GeV} < M_{\ell\ell} < 3100 \text{ GeV}$, one sees a dramatic reduction in the SM background, which amounts to ~ 0.01 fb. The signal, however reduces by a nominal amount to ~ 1.3 fb. Hence, a massive Z' boson has a significant discovery potential during the 14 TeV LHC runs.

¹ A recent study [93] showed the importance of exclusion plots as functions of both masses and couplings.

Searches	Constraints	$M_{Z'}(SSM)$
Boosted $t\bar{t}$ [69]	$\sigma \times B \leq 1 - 2 \text{ pb}$	-
di-lepton-CMS [67]	$R < 7 \times 10^{-6}$	2.90 TeV
di-lepton-ATLAS [66]	$\sigma \times B \leq 4 \times 10^{-2} \text{ pb}$	2.90 TeV
di-jet-ATLAS [68]	$\sigma \times B \times A \leq 0.2 - 0.3 \text{ pb}$	1.70 TeV
$\tau^+\tau^-$ -ATLAS [70]	$\sigma \times B \leq 0.1 \text{ pb}$	1.90 TeV
$b\bar{b}$ -CMS [65]	-	1.20 - 1.68 TeV

TABLE I. The recent bounds on Z' production from di-lepton, di-jet and other analyses.

M_N (TeV)	g'	$M_{Z'}(B-L)$ (TeV)
0.5	0.2	2.62
1.0	0.2	2.65
0.5	0.1	2.25
0.5	0.05	1.83

TABLE II. The bounds on $M_{Z'}$ derived from the ATLAS di-lepton search [66] relevant for a $U(1)_{B-L}$ model.

IV. CONSTRAINTS ON HIGGS MIXING

As discussed in the previous section, the light Higgs, H_1 (or the SM-like Higgs) and the heavy Higgs, H_2 mix with an angle θ . Hence, their couplings to the other particles in the model are scaled accordingly. Before discussing the phenomenological aspects of the searches, we impose bounds on the mixing parameter from the available experimental results. There are further theoretical bounds on this parameter which we discuss below.

- **Experimental bounds :** Recent searches from CMS [74] and ATLAS [75] have already put bounds on a large class of BSM models. We work in the so-called κ framework, where the coupling deviations of the SM-like Higgs are parametrized in terms of simple rescalings. The Higgs coupling to two fermions $g_{H_1 ff}$ and two weak bosons $g_{H_1 VV}$ are defined as [94],

$$g_{H_1 ff} = \kappa_f \cdot g_{H_1 ff}^{\text{SM}} \quad \text{and} \quad g_{H_1 VV} = \kappa_V \cdot g_{H_1 VV}^{\text{SM}}, \quad (22)$$

where κ_f and κ_V are the coupling modifiers and are equal to unity in SM. We quote the 95% CL intervals on the various κ parameters from CMS (Fig. 12 in Ref. [74])

and ATLAS (Fig. 15 in Ref. [75]) in Table III. Here, the experimental collaborations have assumed that the loop level couplings like $H_1 gg$, $H_1 \gamma\gamma$ and $H_1 Z\gamma$ can be parametrized in terms of the tree level couplings and that no new loop particles are involved. They also assume that the invisible branching ratio of H_1 is zero. These assumptions agree with the model under consideration. We consider the mass of heavy neutrinos to be in the TeV scale, for which the SM like Higgs decay to heavy neutrinos is small. In addition, since the light and heavy sterile mixing is small $\sim 10^{-6}$, hence, the SM like Higgs decaying to two light neutrinos is negligible. In this particular model, the couplings $\kappa_t = \kappa_b = \kappa_W = \kappa_Z = \kappa_\tau = \cos\theta$ and can have a maximum value of unity. Thus, all the major production cross-sections for H_1 , e.g. ggF , VBF , VH and $t\bar{t}H$ scale as $\cos^2\theta$.

κ_W	κ_Z	κ_t	κ_b	κ_τ
CMS				
[0.66, 1.24]	[0.69, 1.37]	[0.51, 1.22]	[0.07, 1.46]	[0.47, 1.25]
ATLAS				
[0.63, 1.19]	$[-1.20, -0.67] \cup [0.67, 1.26]$	[0.59, 1.39]	$[-1.29, 1.31]$	$[-1.46, -0.61] \cup [0.62, 1.47]$

TABLE III. The 95% CL ranges on various signal strength modifiers, κ , as reported by CMS [74] and ATLAS [75].

Using the ranges in Table III, we obtain the scale factor of the heavy Higgs, H_2 as $\sin^2\theta < 0.31(0.33)$ for CMS (ATLAS) at 95% CL.

It is however important to note that the bounds on $\sin\theta$ from the coupling measurements of the SM-like Higgs are possibly the most desired and robust ones. These bounds are independent of the mass of the heavy higgs and will probably get more stringent with more integrated luminosity. As an example, in Ref. [95], the $H \rightarrow WW^*$ measurement is shown to constrain $\sin\theta \sim 0.36$ from the projected study of LHC at 14 TeV with $\int \mathcal{L} dt = 300 \text{ fb}^{-1}$. The same study also projects a smaller $\sin\theta \sim 0.25$ at the ILC, running at 250 GeV with an integrated luminosity of 250 fb^{-1} . The ILC runs with greater centre-of-mass energies and higher integrated luminosities are expected to constrain $\sin\theta$ to even smaller values. In this analysis, we assume $\sin\theta = 0.2$ which is in sync with the projected study at LHC 14 with 300 fb^{-1} .

- **Theoretical bounds :**

- **Constraints from M_W :** One of the strongest constraints on the the mixing angle, $\sin\theta$, comes from the one-loop correction to the W -boson mass, M_W , which is required to agree within 2σ of its experimental value, *i.e.*, $M_W = 80.385 \pm 0.015$ GeV [73, 96, 97]. This has recently been studied in the context of this model in Refs. [71, 72, 98]. It has also been shown in Ref. [71], that in the high mass region, the constraints from the one-loop correction to M_W are stronger than the ones obtained from S, T and U parameters [99–102]. The upper bound on $\sin\theta$ decreases from ~ 0.35 to ~ 0.20 as M_{H_2} increases from 250 GeV to 900 GeV [71]. In our analysis, we have considered a conservative value of $\sin\theta = 0.20$, throughout, in order to satisfy all the constraints.
- **Constraints from perturbative unitarity :** Demanding perturbative unitarity [103], by studying all the $2 \rightarrow 2$ scattering amplitudes and demanding that the partial wave amplitudes a_ℓ s follow

$$|\text{Re}(a_\ell)| \leq \frac{1}{2}, \quad (23)$$

where the subscript ℓ denotes the orbital angular momentum, results in an upper bound on the Higgs boson mass. The bounds from perturbative unitarity for a model with a scalar extension has been derived in Ref. [104]. Perturbative unitarity also poses strong constraints on the ratio $\tan\beta = v/v'$.

- **Perturbativity of the couplings :** All the couplings in the potential are required to conform within perturbative limits, *i.e.*, $\lambda_{1,2,3} \leq 4\pi$. These bounds are weaker than the ones obtained from perturbative unitarity at the EW scale. Besides, constraints from vacuum stability and the renormalisation group evolution of $\lambda_{1,2,3}$ are also studied in Refs. [62, 71, 105].

V. COLLIDER SEARCHES FOR THE HEAVY HIGGS

The heavy Higgs H_2 in the $B - L$ model mixes with the SM-like Higgs, H_1 , with mixing angle θ , as has been discussed in the previous sections. H_2 can be produced at the LHC through multiple production processes, e.g. gluon fusion (ggF), weak boson fusion (VBF), associated WH_2/ZH_2 productions and the associated $t\bar{t}H_2$ production mode. Once produced, H_2 promptly decays into different final states, with WW , H_1H_1

and ZZ being the dominant decay modes. In this section, we study in detail the collider signatures of H_2 produced through its dominant production mode, ggF , after including the constraints on the mixing angle, θ , as discussed above. In order to study the collider signatures of H_2 , we implement the model using `FeynRules` [106]. The generated `Universal FeynRules Output` (UFO) [107] files are then fed to the Monte-Carlo (MC) event generator `MadGraph` [108] for generation of event samples. The parton-showering and hadronisation is carried out in the `Pythia 6` [109] framework. For jet formation, we use the anti- k_T algorithm with a jet parameter of $R = 0.4$ [110].

In Fig. 2a we show the branching ratios of H_2 to various final states as function of its mass, varying M_{H_2} between 250 GeV and 1 TeV. As is clear from Fig. 2a, the three most dominant decay modes of H_2 are WW , H_1H_1 and ZZ . In Fig. 2b, we show the Next-to-Next-to Leading Order (NNLO) cross-sections of the three different final states mentioned above. Note that, in addition to the aforementioned processes, we also show the cross-section for the process $pp \rightarrow H_2 \rightarrow WW \rightarrow 2\ell\not{E}_T$ in Fig. 2b. However, we do not consider the phenomenology for the latter process because of a somewhat less amount of handle on its kinematics due to fewer visible particles in the final state. The cross-section of H_2 decaying to $\ell\nu 2j$ is the highest, whereas for the 4ℓ channel, the cross-section is the smallest. We analyze these two channels in considerable details and study the discovery prospects of H_2 at the HL-LHC. We also briefly mention the $2\ell 2j$ final state as a potential channel for discovering H_2 .

Recently, search strategies for $H_2 \rightarrow H_1H_1$ have been discussed in Refs. [98, 111–114]. CMS [115] and ATLAS [116, 117] have studied the di-higgs production in the $b\bar{b}b\bar{b}$ and $b\bar{b}\gamma\gamma$ final states mostly in the context of models with extra spatial dimensions. The upper limits on $\sigma \times B$ for the resonant and non-resonant production of di-higgs in context of such BSM models are found in Refs. [115–117]. A naive leading order estimate of the $pp \rightarrow H_1H_1$ cross-sections [118] with $v' = 3.75$ TeV and $\sin\theta = 0.2$ reveals that for lower values of M_{H_2} , *i.e.*, up to ~ 500 GeV, the cross-section is substantially enhanced with respect to the SM cross-section. However, with higher values of M_{H_2} , H_2 decouples and the cross-section tends to the SM value, see Fig. 3. Hence, this channel can complement the gauge-boson final states in searches for H_2 .

In the present work, we focus on the WW and ZZ decay modes and try to devise some search strategies in the context of the 14 TeV run at the HL-LHC. Although, the branching ratios of W/Z decaying to di-jet final states are large, still, the leptonic and

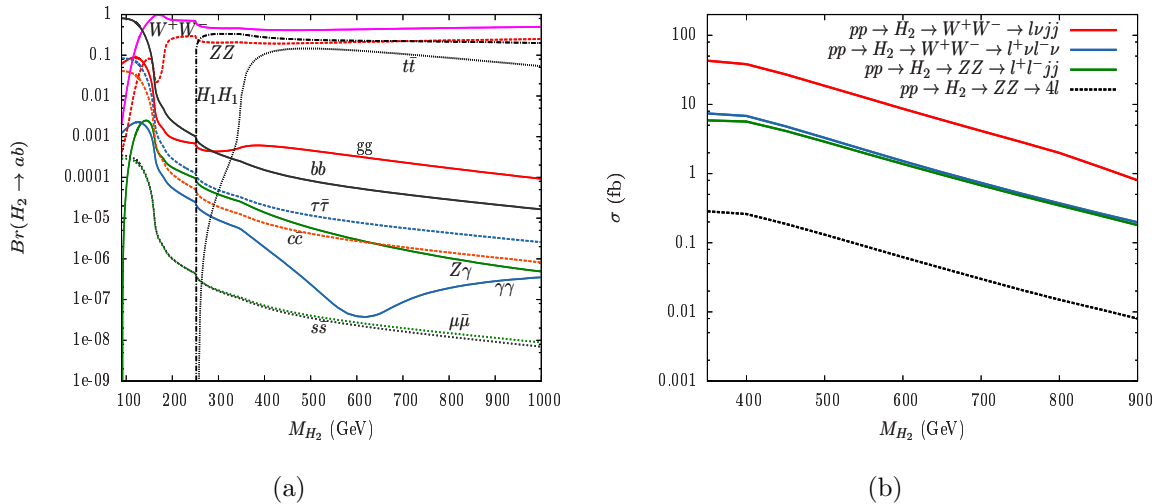


FIG. 2. Left panel : Branching ratios of H_2 (as a function of M_{H_2}) to W^+W^- (solid magenta), ZZ (dotted red), H_1H_1 (dot-dashed black), $t\bar{t}$ (dotted black), $b\bar{b}$ (solid black), gg (solid red), $\tau\bar{\tau}$ (dotted blue), $Z\gamma$ (solid green), $c\bar{c}$ (fine-dotted red), $\gamma\gamma$ (solid blue), $\mu\bar{\mu}$ (fine-dotted green) and $s\bar{s}$ (fine-dotted black). Right panel : NNLO Cross section (fb) times Branching ratio as functions of M_{H_2} ($pp \rightarrow H_2 \rightarrow W^+W^- \rightarrow \ell\nu jj$ [solid red], $pp \rightarrow H_2 \rightarrow W^+W^- \rightarrow \ell^+\nu\ell^-\nu$ [solid blue], $pp \rightarrow H_2 \rightarrow ZZ \rightarrow \ell^+\ell^- jj$ [solid green] and $pp \rightarrow H_2 \rightarrow ZZ \rightarrow 4\ell$ [dotted black]). $\sin\theta = 0.2$ for all the cases.

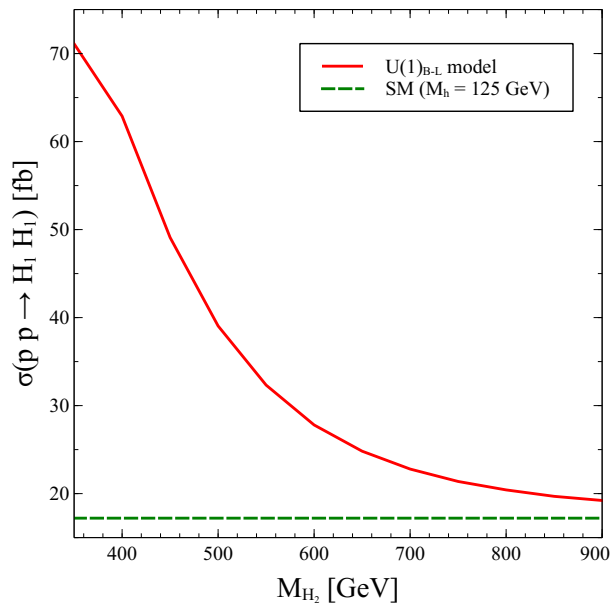


FIG. 3. LO cross-section for the channel $pp \rightarrow H_1H_1$ for (a) the $U(1)_{B-L}$ model (solid red curve) and (b) the SM with $M_h = 125$ GeV (green curve).

semi-leptonic decay modes offer the cleanest possible signatures because of significantly less backgrounds. Therefore, in our subsequent discussions, we concentrate only on those channels, that have leptons in the final state, i.e.

- $pp \rightarrow H_2 \rightarrow ZZ \rightarrow 4\ell$,
- $pp \rightarrow H_2 \rightarrow ZZ \rightarrow 2j2\ell$ and
- $pp \rightarrow H_2 \rightarrow WW \rightarrow l\nu 2j$

For the search strategies, we adopt two different reconstruction methods which we discuss below.

- **Cut-based analysis (CBA)** : In this method, we employ rectangular cuts on various kinematic variables in order to optimise the significance

$$n = \mathcal{N}_S / \sqrt{\mathcal{N}_S + \mathcal{N}_B} .$$

- **Multivariate analysis (MVA)** : We employ multivariate techniques for better signal-to-background discrimination, resulting in better signal significance, n . For the present study, we use the Boosted Decision Tree (BDT) algorithm from the TMVA [119] framework. In order to perform an MVA, we select the set of kinematic variables that give the maximum discrimination between signal and background. Both the signal and backgrounds are trained by this algorithm and another set of event samples are used to test the BDT output. For any MVA, we must always be alert not to over-train signal and background. The universally accepted Kolmogorov-Smirnov (KS) test can reveal if our choice of parameters needs to be changed. The test sample is not over-trained if the KS probability lies in the range (0.1, 0.9). For most cases, a critical value of the KS probability greater than 0.01 [120] implies that the samples are not over-trained. For the subsequent studies we ensure that over-training is not an issue over the entire parameter range. In order to estimate the LHC's potential in excluding H_2 , we use the result of the MVA as input to a binned log-likelihood hypothesis test [121].

In the following subsections we discuss the discovery prospects of the heavy higgs.

A. $pp \rightarrow H_2 \rightarrow ZZ \rightarrow 4\ell$

In this scenario, H_2 is produced on-shell and decays to two Z bosons. The two Z bosons subsequently decay to four leptons. The main background for this process is the ZZ production mode that will generate the same final state. To analyse this channel we employ the following trigger cuts:

• Trigger Cuts (TC):

To identify the leptons, we apply the following minimal cuts.

1. Transverse Momentum: $p_T(l) > 10$ GeV
2. Pseudo-rapidity: $|\eta(l)| < 2.5$
3. Radial Distance: $\Delta R(l_i, l_j) > 0.2$

We show the normalised distributions of various kinematic variables in Figs. 4 and 5 for $M_{H_2} = 250, 500$ and 900 GeV with respect to the background. It is evident from Fig. 5a, that while for the signal, the invariant mass of four leptons peaks at the heavy Higgs mass, M_{H_2} , this is not true for the background and hence serves as one of the better discriminating variables. The leptons originating from the Z decays also have higher transverse momentum compared to the background, which peaks at lower p_T values. The two Z bosons also have higher p_T with respect to the background, as shown in Figs. 5b and 5c. For higher M_{H_2} , both the Z s have $p_T > 100$ GeV. For our cut-based analysis (CBA), we use these following selection cuts to separate signal from background to a good degree.

• Selection Cuts (SC)

We use the following selection cuts:

1. Invariant mass of the four lepton system: $M_{4\ell}$ to lie in the range, $M_{H_2} \pm 10$ GeV
2. Transverse momentum of leading lepton: $p_{T_{\ell_1}} > 90$ GeV
3. Transverse momentum of sub-leading lepton: $p_{T_{\ell_2}} > 70$ GeV
4. Transverse momentum of the other two leptons: $p_{T_{\ell_3}} > 50$ and $p_{T_{\ell_4}} > 20$ GeV
5. Invariant mass of the reconstructed Z bosons: $M_{Z_1}, M_{Z_2} \in M_Z \pm 10$ GeV
6. Transverse momentum of the two reconstructed Z bosons: $p_T(Z_1), p_T(Z_2) > 100$ GeV

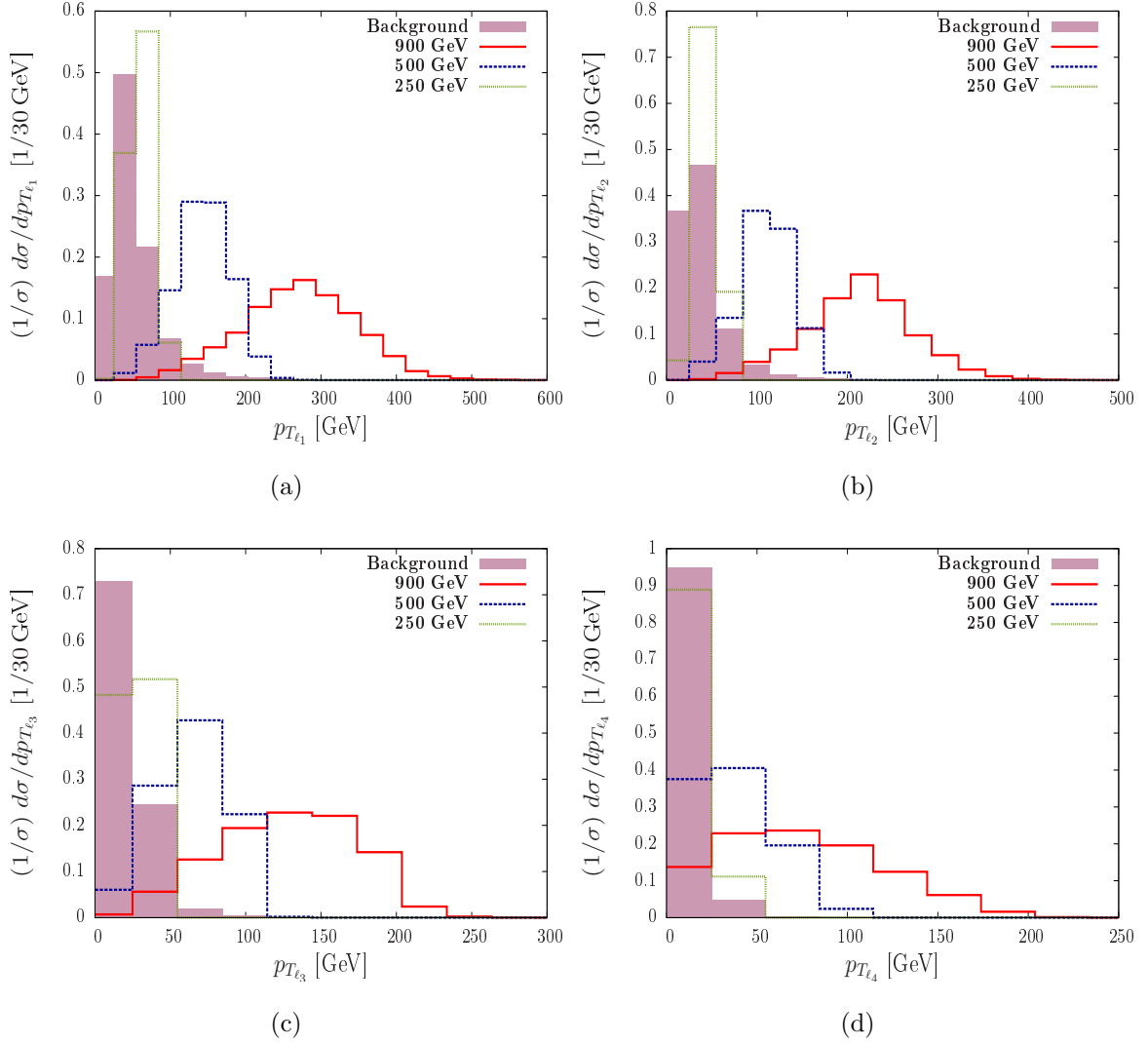


FIG. 4. $pp \rightarrow ZZ \rightarrow 4\ell$ channel normalised distributions for $M_{H_2} = 250 \text{ GeV}$ (green dotted line), 500 GeV (blue dashed line), 900 GeV (red solid line) and background (purple solid): (a)-(d) p_T distributions of the four leptons, p_T sorted.

For the MVA analysis, we choose a set of 18 kinematic variables with the maximum discriminating power, which are $M_{4\ell}$, $p_{T_{\ell_i}}$, $\Delta R_{\ell_i \ell_j}$, M_{Z_k} , $p_T(Z_k)$, $\eta(Z_k)$ and $p_T(4\ell)$. Here $i, j = 1, 4$, $k = 1, 2$ and the leptons and two Z s are p_T sorted. $p_T(4\ell)$ is the vector sum of p_T of the four leptons.

We tabulate the signal and background cross-sections after the trigger cuts (TC) and the selection cuts (SC) in Table. IV for M_{H_2} in the range $300 - 700 \text{ GeV}$. We also list the number of signal (\mathcal{N}_S) and background (\mathcal{N}_B) events computed for an integrated luminosity of 3000 fb^{-1} for the cut-based and BDT analyses after imposing the respective cuts. Fig. 6 shows the normalised distributions for the signal and the background against the BDT response for two benchmark masses, $M_{H_2} = 250 \text{ GeV}$ and 500 GeV . We find that with

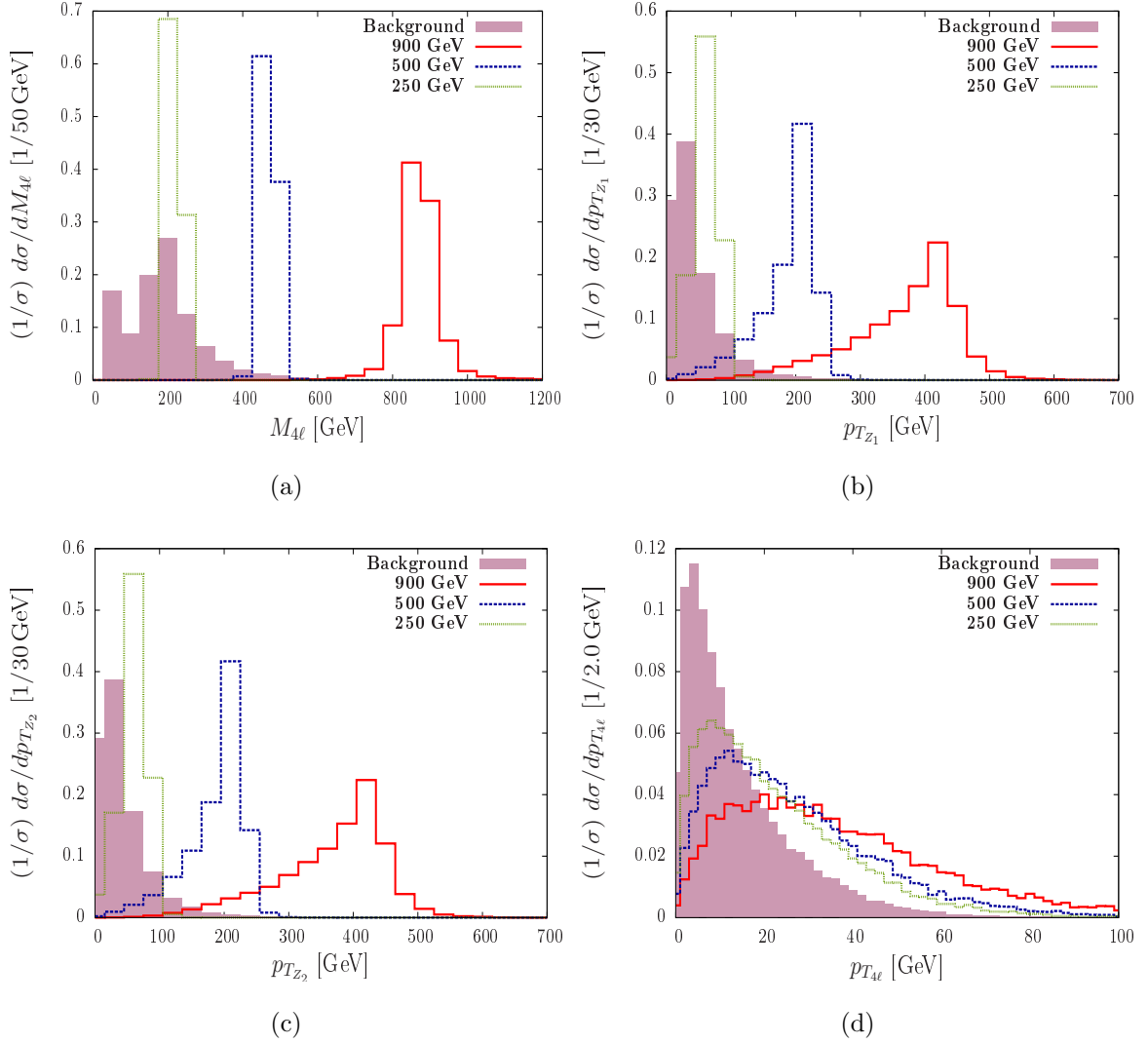


FIG. 5. $pp \rightarrow ZZ \rightarrow 4\ell$ channel normalised distributions for $M_{H_2} = 250$ GeV (green dotted line), 500 GeV (blue dashed line), 900 GeV (red solid line) and background (purple solid): (a) invariant mass of the four leptons, (b)-(c) transverse momenta of the two reconstructed Z bosons and (d) vector sum p_T of the four lepton system.

an increase in mass, the overlap between the signal and the background decreases. As a result, using a BDT, S/B improves significantly.

The maximum significance is obtained for relatively small masses of H_2 , where the cross-sections are sufficiently large. Note that, even with the cut-based analysis, the discovery prospect of the heavy Higgs is rich for 3000 fb^{-1} integrated luminosity. As an example, with the cut-based analysis, a Higgs with mass $M_{H_2} = 400$ GeV can be discovered with 8.6σ significance (n_{CBA}) at the HL-LHC with an integrated luminosity of 3000 fb^{-1} . As expected, the BDT analysis is seen to improve the significance (n_{BDT})

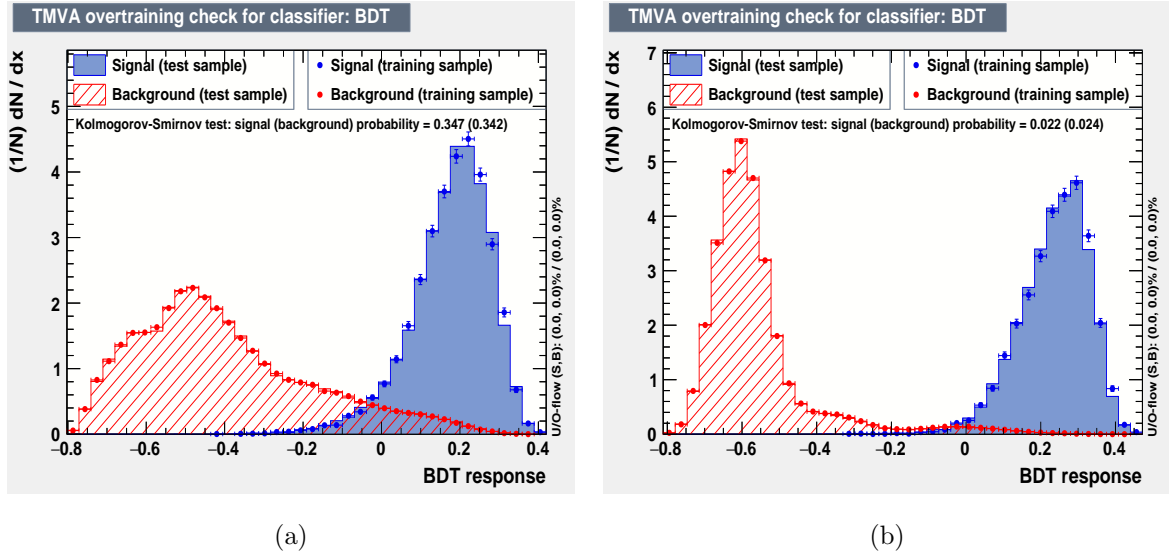


FIG. 6. Normalised signal and background distributions against BDT response for (a) $M_{H_2} = 250$ GeV and (b) $M_{H_2} = 500$ for the channel $pp \rightarrow H_2 \rightarrow ZZ \rightarrow 4\ell$.

by a considerable amount. In the entire mass spectrum, the maximum difference in n_{CBA} and n_{BDT} occurs for $M_{H_2} = 300$ GeV, where the signal and background distributions mostly overlap, making it very difficult to impose rectangular cuts.

To estimate the necessary integrated luminosity to exclude the existence of the heavy Higgs boson, we use the BDT output, shown in Fig. 6, weighted with the according cross section as input for a CLs likelihood ratio [121], see Fig. 7. Conservatively, we assume a flat systematic uncertainty of 10% for each bin. While an H_2 with $M_{H_2} = 250$ GeV can be excluded at 95% CL with 100 fb^{-1} in this channel, excluding $M_{H_2} = 700$ GeV requires 3000 fb^{-1} .

B. $pp \rightarrow H_2 \rightarrow ZZ \rightarrow 2\ell + 2j$

The channel $H_2 \rightarrow ZZ \rightarrow 2l2j$ has been studied in [122] in the context of heavy SM Higgs boson searches. While the signal benefits from a larger branching ratio of the Z boson to jets compared to leptons, the only major background in this channel remains continuum ZZ production. Here, for convenience, we briefly describe the selection cuts discussed in full detail in Ref. [122].

- **Leptonic Z reconstruction :** We demand two isolated muons with $p_T > 15$ GeV and $|\eta| < 2.5$. We further demand an invariant mass window of 10 GeV around M_Z .

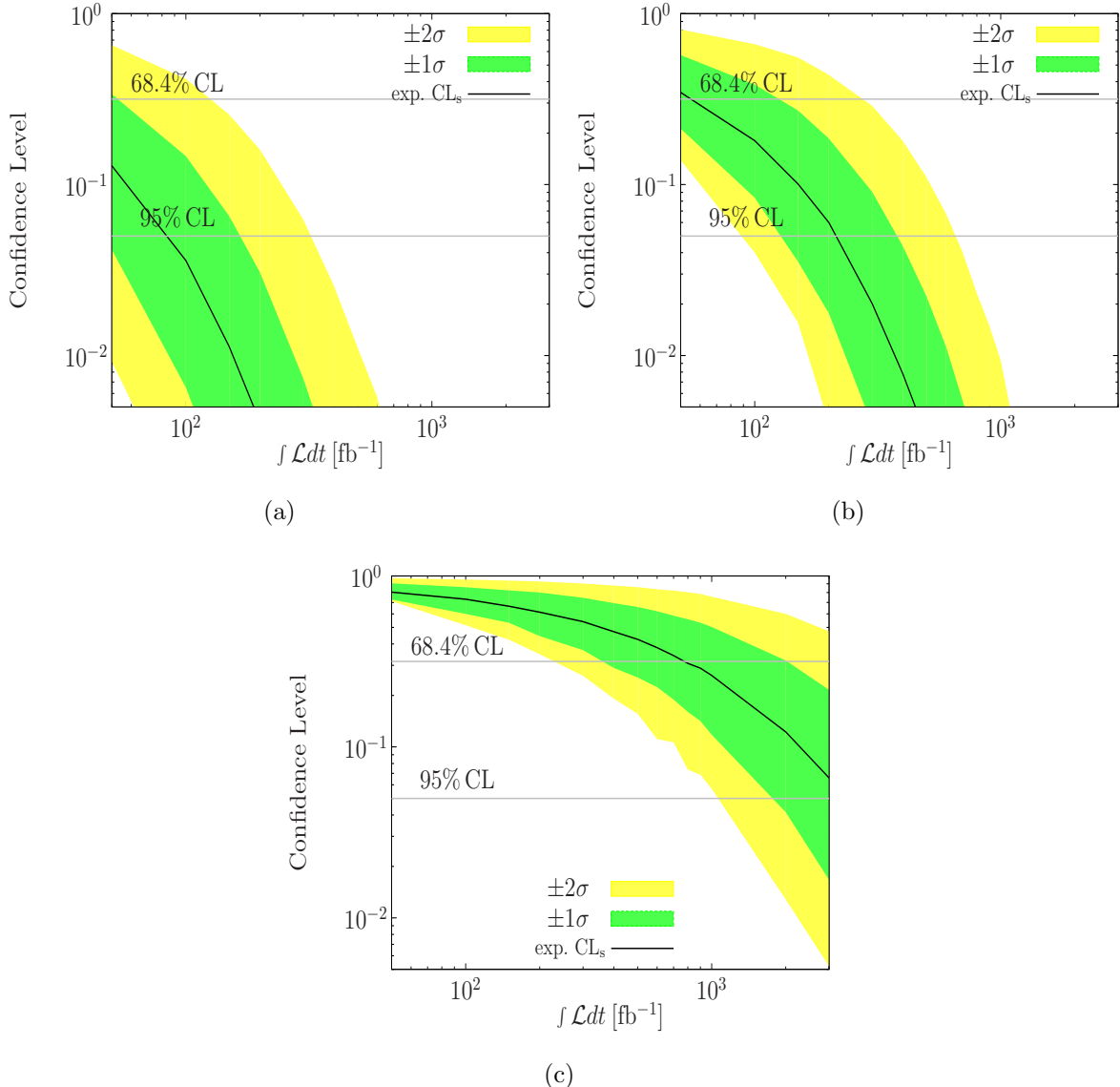


FIG. 7. Confidence level contours for $M_{H_2} =$ (a) 250 GeV, (b) 500 GeV and (c) 700 GeV. We show results for integrated luminosities ($\int \mathcal{L} dt$) from 50 to 3000 fb^{-1} . We assume a flat systematic uncertainty on the backgrounds of 10%.

- **Hadronic Z reconstruction :** We reconstruct the hadronic Z following the algorithm given in Ref. [123]. Here also we require an invariant mass window of 10 GeV around M_Z .
- **Heavy Higgs reconstruction :** If the previous two steps are successfully satisfied, then the invariant mass peaks as $M_{H_2}^2 = (p_{Z_{lep}} + p_{Z_{had}})^2$, where $p_{Z_{lep}}$ and $p_{Z_{had}}$ are respectively the four-momenta of the reconstructed Z bosons in the leptonic and hadronic channels. The Higgs mass windows used for the four benchmark masses are $(300 \pm 30, 350 \pm 50, 400 \pm 50, 500 \pm 70, 600 \pm 100)$ GeV. These are found to

M_{H_2} (GeV)	σ^{TC} (fb)	σ^{SC} (fb)	\mathcal{N}_S^{CBA}	\mathcal{N}_B^{CBA}	n_{CBA}	\mathcal{N}_S^{BDT}	\mathcal{N}_B^{BDT}	n_{BDT}
300	0.126	0.010	30	105	2.62	227	555	8.12
350	0.132	0.042	125	162	7.37	262	419	10.03
400	0.113	0.047	142	131	8.60	246	361	9.99
450	0.078	0.034	101	101	7.14	168	243	8.29
500	0.051	0.021	63	81	5.26	93	132	6.19
550	0.034	0.013	40	48	4.23	54	70	4.82
600	0.022	0.008	24	45	2.87	42	112	3.42
650	0.015	0.005	14	32	2.12	23	60	2.54
700	0.010	0.003	9	24	1.57	16	87	1.58
SM	28.626	-	-	-	-			

TABLE IV. NNLO cross sections after trigger cuts (σ^{TC}) and selection cuts (σ^{SC}). \mathcal{N}_S and \mathcal{N}_B represent the number of signal and background events, respectively, while the superscript and subscripts CBA and BDT represent the cut-based and BDT analysis. n is the significance. The number of events have been computed for an integrated luminosity 3000 fb^{-1} . All the cross-sections include the higher order corrections to the NNLO level.

optimise the results. Also because the Higgs width increases significantly with M_{H_2} , we widen the windows for reconstruction purposes.

- **ZZ separation** : To further improve S/B , we require the leptonic and hadronic Z bosons to have a maximum isolation of $\Delta R_{ZZ} < 3.2$, where $\Delta R = \sqrt{\Delta\eta^2 + \Delta\phi^2}$ with $\Delta\eta$ and $\Delta\phi$ being the separation between two objects in the pseudo-rapidity and azimuthal angle planes respectively. For $Z + \text{jets}$, ΔR between the reconstructed Z_{lep} and the fake- Z from the QCD jets often becomes large in order to account for the large Higgs invariant mass.
- **Pruning and trimming** : The pruning [124, 125] and trimming [126] algorithms are used to further reduce the QCD backgrounds because this technique helps in discriminating colour singlet resonances from QCD jets [127]. The details of this procedure are elucidated in Ref. [122].

After assuming $\sin\theta = 0.2$ and applying the reconstruction outlined in [122] we find the results shown in Tab. V.

M_{H_2} (GeV)	$\sigma_{SC}^{ggF+VBF}$ (fb)	σ_{SC}^{bkg} (fb)	S/B	$S/\sqrt{S+B}_{100}$	$S/\sqrt{S+B}_{3000}$
300	0.048	2.10	0.023	0.331	1.811
400	0.290	19.21	0.015	0.657	3.602
500	0.223	18.01	0.012	0.522	2.858
600	0.121	11.83	0.010	0.351	1.920

TABLE V. $\sigma_{SC}^{ggF+VBF}$ is the production cross-section of H_2 from the ggF and VBF channels combined after employing the selection cuts discussed in Ref. [122]. σ_{SC}^{bkg} is the background cross-section for the same set of selection cuts. The table also shows the discovery potential of H_2 in this channel with the help of S/B and $S/\sqrt{S+B}$. The subscripts 100 and 3000 imply the significance computed at the respective integrated luminosities in fb^{-1} .

Hence, the sensitivity in the $H_2 \rightarrow 2\ell 2j$ channel alone is fairly small for the $U(1)_{B-L}$ model, based on the reconstruction of boosted Z bosons. However, this channel can be combined with the other channels in a global fit.

C. $pp \rightarrow H_2 \rightarrow WW \rightarrow \ell + \cancel{E}_T + \geq 2j$

In this scenario, H_2 decays to W^+ and W^- , followed by the subsequent decay of one of the W s to a lepton and missing energy and the other one to a pair of jets.

Recently, the ATLAS collaboration has searched for WW/WZ resonances decaying to a lepton, neutrino and jets [128], that mimic our signal. With a $p_T(W) > 400$ GeV cut, used in Ref. [128], our signal cross-sections will be extremely small. In Ref. [128], the authors have considered two benchmark models, *viz.*, (i) a spin 2 Kaluza-Klein Graviton for the WW resonance and (ii) a spin-1 SSM W' decaying to a WZ pair. From Fig. 2b, we find that the production cross-section of $pp \rightarrow H_2 \rightarrow W^+W^-$ is approximately $\sigma \leq 0.098$ pb, that is way below the exclusion limit, as given in Fig. 2 of Ref. [128]. Hence, we adopt different sets of cuts which are suitable for our analysis.

For a heavy Higgs boson, the intermediate W s are expected to have large p_T . Because the W bosons are highly boosted, the leptons and jets are expected to have a large isolation of $\Delta R(l, j_i)$. We show the normalised distributions of various kinematic variables in Figs. 8, 9, 10 and 11, for the masses $M_{H_2} = 250, 500, 900$ GeV and for the SM

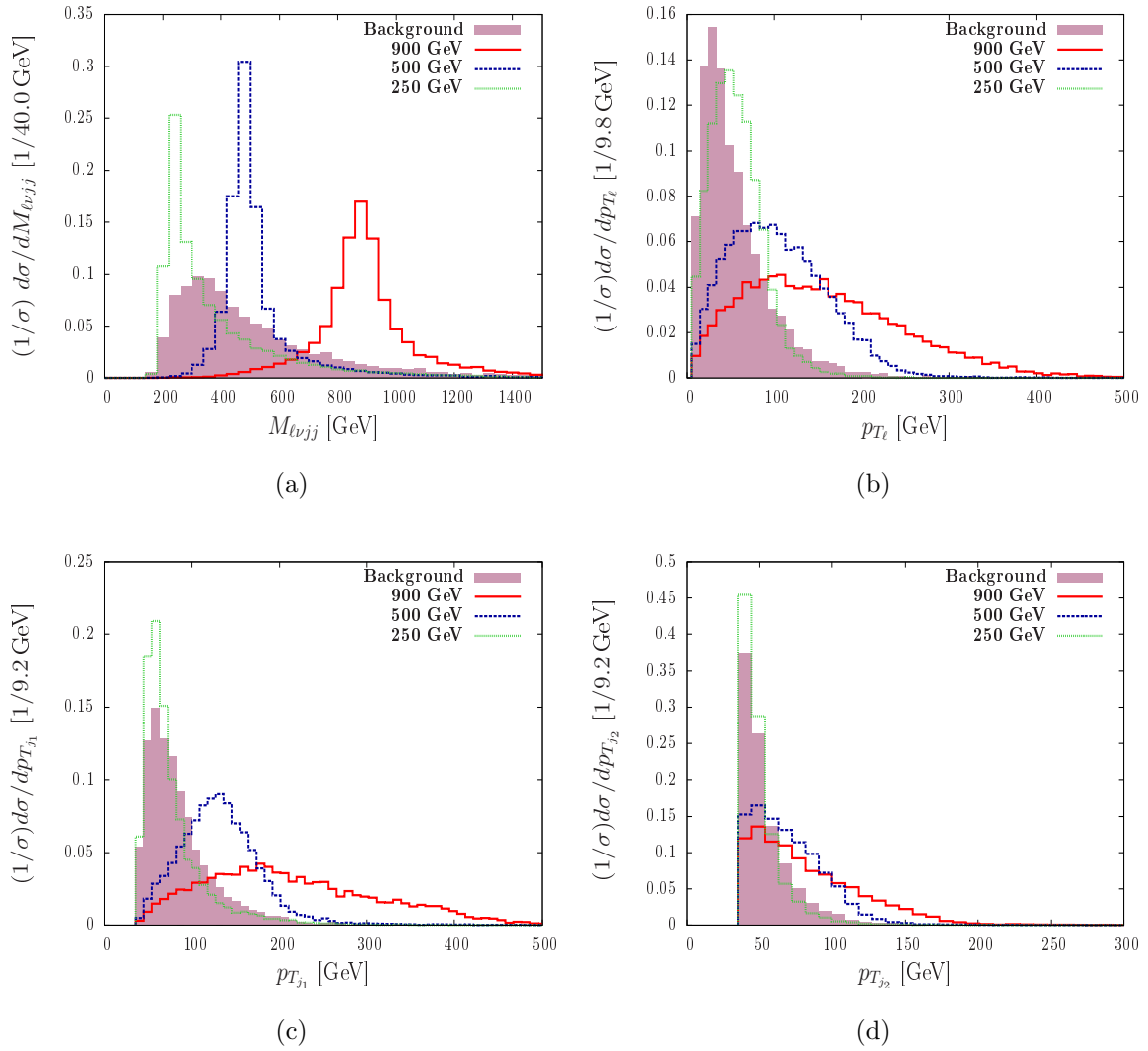


FIG. 8. $pp \rightarrow WW \rightarrow \ell 2j \cancel{E}_T$ channel normalised distributions for $M_{H_2} = 250$ GeV (green dotted line), 500 GeV (blue dashed line), 900 GeV (red solid line) and background (purple solid): (a) Invariant mass of $\ell 2j \cancel{E}_T$, (b) p_T of lepton, (c)-(d) p_T of the two tagged jets.

background.

To identify the leptons and jets, we apply the following minimal cuts:

- **Trigger Cuts (TC)**

1. Transverse Momentum of the jets : $p_T(j_i) > 30$ GeV, where i is the jet-index
2. Transverse Momentum of the lepton : $p_T(l) > 20$ GeV
3. Pseudo-rapidity of the lepton : $|\eta(l)| < 2.5$
4. Pseudo-rapidity of the jets : $|\eta(j_i)| < 5.0$
5. Radial Distance between jets i and j : $\Delta R(j_i, j_j) > 0.4$

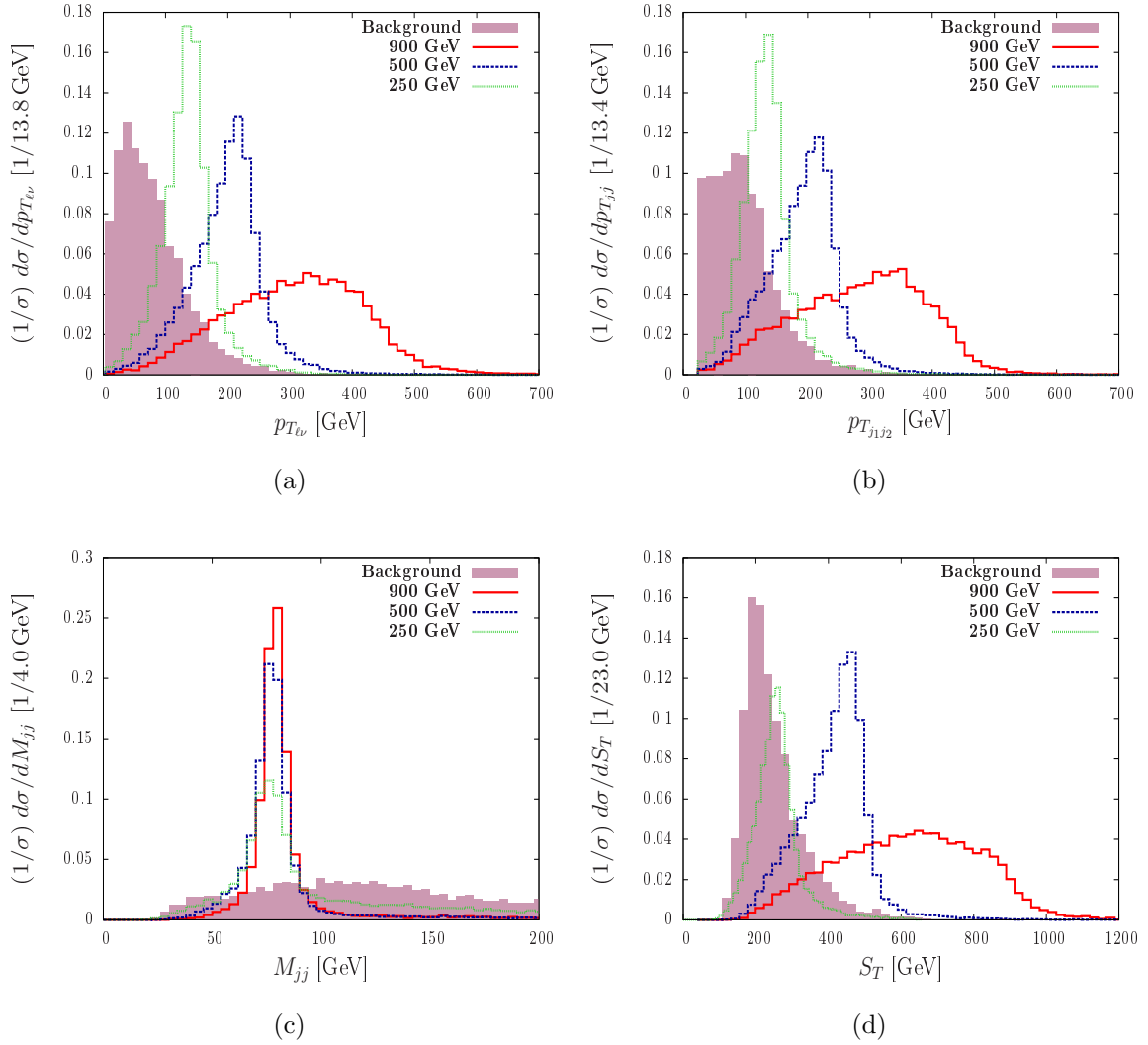


FIG. 9. $pp \rightarrow WW \rightarrow \ell 2j \cancel{E}_T$ channel normalised distributions for $M_{H_2} = 250$ GeV (green dotted line), 500 GeV (blue dashed line), 900 GeV (red solid line) and background (purple solid): (a) p_T of the $\ell\nu$ system, (b) p_T of the di-jet system which reconstructs the W mass, (c) Invariant mass of di-jet system which reconstructs the W mass, (d) scalar sum p_T of lepton, two-tagged jets and \cancel{E}_T .

6. Radial Distance between lepton and the i^{th} jet: $\Delta R(l, j_i) > 2.0$

In the above, j_1 and j_2 denote two leading jets, sorted according to their transverse momentum. For the Higgs masses, M_{H_2} of our interest, both the intermediate gauge bosons are on-shell and this allows us to fully reconstruct them. For the hadronically decaying W , we use the jet four-momentum, while for the leptonically decaying W , we fix the longitudinal component of the neutrino momentum, $p_z(\nu)$ by imposing the constraint $M_W^2 = (p_l + p_\nu)^2$.

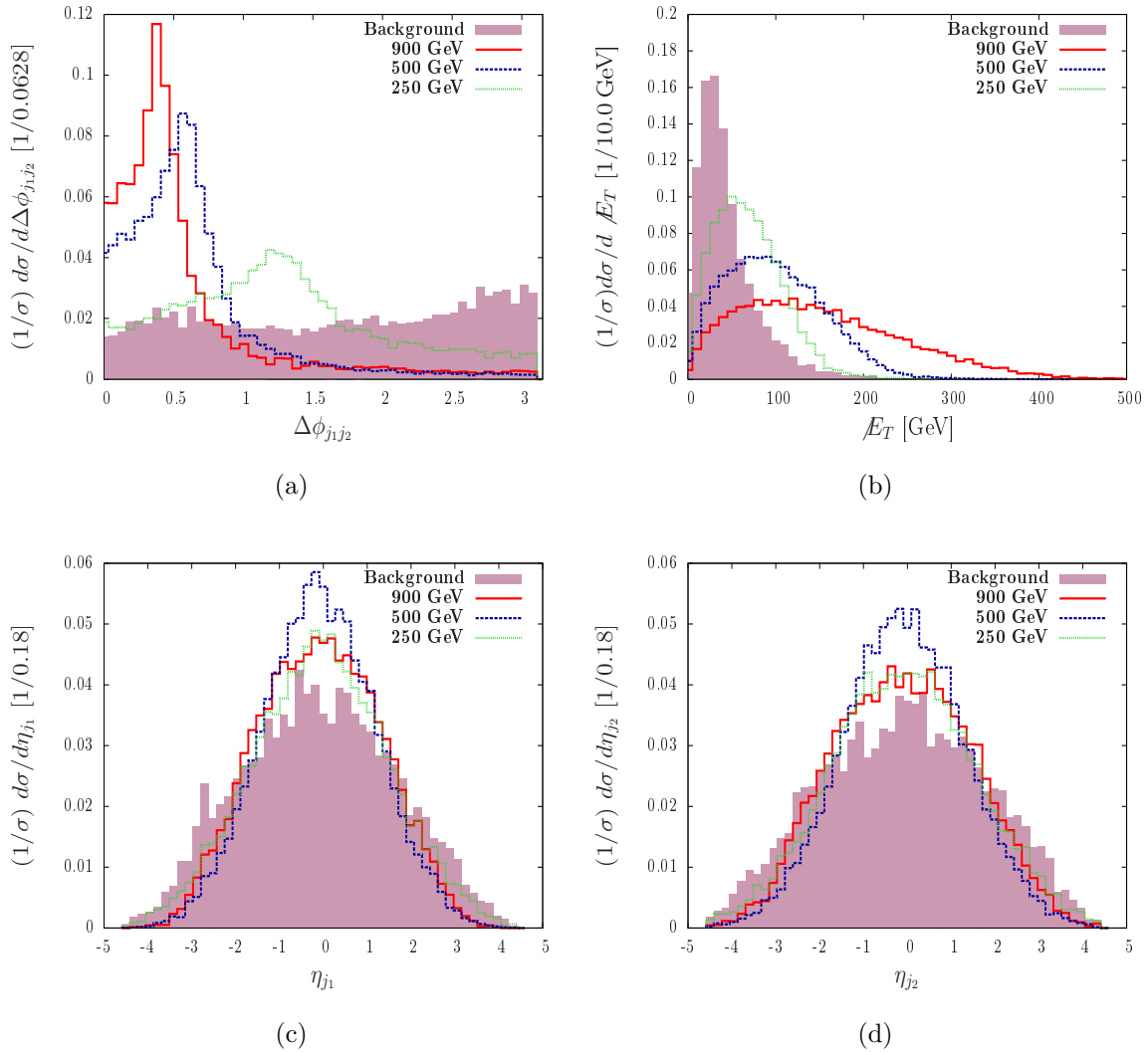


FIG. 10. $pp \rightarrow WW \rightarrow \ell 2j \cancel{E}_T$ channel normalised distributions for $M_{H_2} = 250$ GeV (green dotted line), 500 GeV (blue dashed line), 900 GeV (red solid line) and background (purple solid): (a) $\Delta\phi_{j_1j_2}$ between the two tagged jets, (b) \cancel{E}_T , (c) pseudorapidity of the hardest p_T jet, (d) pseudorapidity of the second hardest p_T jet and (e) pseudorapidity of the lepton.

The major part of the background originates from non-resonant W^+W^- production, with one W decaying hadronically and the other decaying leptonically. From the different p_T distributions in Figs. 8 and 9, it is evident that for low masses, the signal and background has large overlap, making the discrimination a difficult task. In addition, for the invariant mass, $lj\cancel{E}_T$, the signal and background show a large overlap for $M_{H_2} \approx 250$ GeV (see Fig. 8a), whereas for larger masses, the overlap decreases. p_T of the lepton and the leading-jet are large for $500 \text{ GeV} < M_{H_2} < 900 \text{ GeV}$. We also show the transverse momentum of the two reconstructed W s in Figs. 9a and 9b. For the signal, they peak at

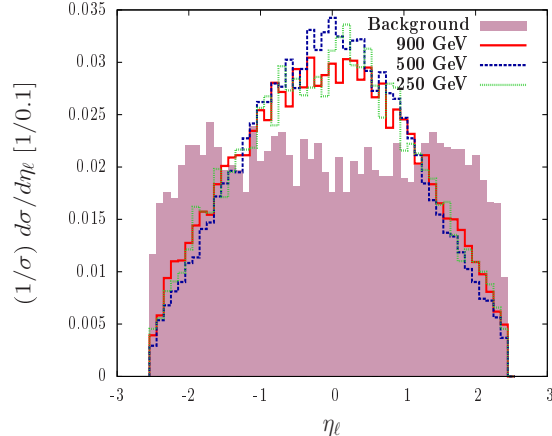


FIG. 11. $pp \rightarrow WW \rightarrow \ell 2j \cancel{E}_T$ channel normalised distributions for $M_{H_2} = 250$ GeV (green dotted line), 500 GeV (blue dashed line), 900 GeV (red solid line) and background (purple solid): pseudorapidity of the lepton.

$p_T(W) > 100$ GeV, while for the background, most of the intermediate W s have lower p_T . In addition, the signal has a large missing transverse energy (\cancel{E}_T), as evident from Fig. 10b. In Fig. 9c, we show the invariant mass distribution of the two hardest jets and in Fig. 10a we show the distribution of their azimuthal angle separation.

Note that the partonic signal cross-section, σ_{sig} varies from few tens of fb to $\mathcal{O}(0.1)$ fb, for M_{H_2} varying between 300 GeV and 900 GeV. However, the background for this process is extremely large $\sigma_{\text{bkg}} \sim 3380$ pb. Hence, to extract the signal from background in a statistically viable fashion, we categorise the signals into four separate regions and implement stringent cuts both at the generation level as well as at the detector level.

M_{H_2} (GeV)	$p_T(l/j_1/j_2)$ (GeV)	$\Delta R(j_1, j_2)_{\text{min}}$	$\Delta R(j_1, j_2)_{\text{max}}$	\cancel{E}_T (GeV)
350	30	0.4	1.4	50
500	40	0.2	1.0	60
700	50	0.2	0.8	70
900	70	0.2	0.6	90

TABLE VI. Basic trigger cuts used to separate the signal from background in the $pp \rightarrow H_2 \rightarrow WW \rightarrow \ell + \cancel{E}_T + \geq 2j$ channel.

- The low mass region: $M_{H_2} \sim 350$ GeV case: For this case the signal and background has a large overlapping region. The transverse momentum variable for the lepton

M_{H_2} (GeV)	$p_{T,l/j_{1,2}}$ (GeV)	$p_{T,W_{1,2}}$ (GeV)	$\Delta R_{j_1,j_2}^{\max}$	\cancel{E}_T (GeV)	S_T (GeV)	$ M_{ljj\cancel{E}_T} - M_{H_2} $ (GeV)	$ M_{jj} - M_W $ (GeV)
350	35	100	1.35	55	225	50	20
500	45	100	0.9	70	250	50	20
700	55	100	0.75	75	250	50	20
900	75	100	0.58	95	600	50	20

TABLE VII. Selection cuts to separate out signal from the background in the $pp \rightarrow H_2 \rightarrow WW \rightarrow \ell + \cancel{E}_T + \geq 2j$ channel.

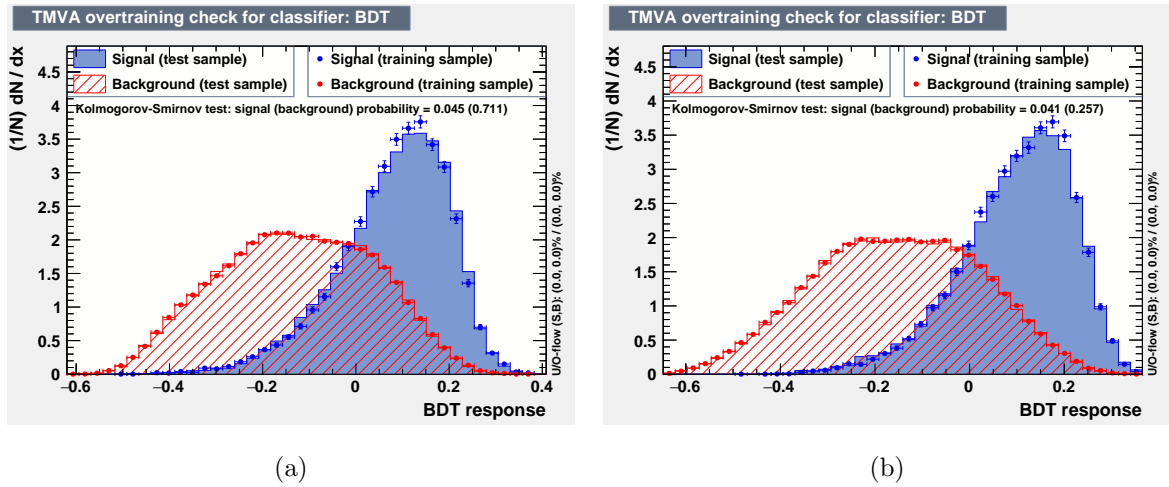


FIG. 12. Normalised signal and background distributions against BDT response for (a) $M_{H_2} = 350$ GeV and (b) $M_{H_2} = 500$ for the channel $pp \rightarrow H_2 \rightarrow WW \rightarrow \ell\nu jj$.

and jets peak around 30 GeV for the background. Hence, to reduce the background, we implement selection cuts, such as, $p_T > 35$ GeV, missing transverse energy $\cancel{E}_T > 55$ GeV and the scalar sum of transverse momentum of the $\ell\nu jj$ system, $S_T > 225$ GeV. In addition, the selection cuts on the invariant mass of the $\ell\nu jj$ system, $|M_{\ell\nu jj} - M_{H_2}| = 50$ GeV reduces the background significantly.

- Intermediate mass range: $M_{H_2} \sim 500$ GeV: For the intermediate mass range, such as, $M_{H_2} = 500$ GeV, the signal and background has a relatively smaller overlap, as is evident from Figs. 8b, 8c and 8d. In addition, the reconstructed W s have large transverse momenta, as shown in Figs 9a and 9b. The invariant mass of the $\ell\nu jj$ system peaks around 500 GeV, while for background the invariant mass peaks at much lower values. The larger cuts on the transverse momenta of the W s and

M_{H_2} (GeV)	σ_s (fb)	σ_{bkg} (pb)	σ_s^{SC} (fb)	σ_{bkg}^{SC} (fb)	$\mathcal{N}_{S_{100}}^{CBA}$	$\mathcal{N}_{B_{100}}^{CBA}$	$\mathcal{N}_{S_{3000}}^{CBA}$	$\mathcal{N}_{B_{3000}}^{CBA}$
350	16.85	24.22	5.49	1666.29	549	166629	16474	4998880
500	9.06	6.69	3.44	360.26	344	36026	10305	1080769
700	2.39	2.56	0.84	77.63	84	7763	2509	232887
900	0.57	0.65	0.06	6.19	6	619	193	18564

TABLE VIII. The NNLO signal (σ_s) and background (σ_{bkg}) cross-sections and the number of events for different Higgs masses. The $\mathcal{N}_{S_{100}/B_{100}}^{CBA}$, $\mathcal{N}_{S_{3000}/B_{3000}}^{CBA}$ are the signal and background events with 100 and 3000 fb $^{-1}$ integrated luminosities for the cut based analysis.

the cuts on the invariant mass efficiently reduces the background cross-section from ~ 3380 pb to ~ 6.69 pb.

- Large masses: $M_{H_2} \sim 700$ GeV: For large masses, such as, $M_{H_2} = 700$ GeV, the signal cross-section after the selection cuts is relatively small $\sigma \sim 0.84$ fb. However, the background is well separated. Hence, the stringent cuts on the kinematic variables improves the sensitivity. We use larger cuts on the transverse momenta of the lepton, jets and the reconstructed W s, as shown in Tables VI and VII. The background cross-section after the different trigger and selection cuts reduce to ~ 2.56 pb.
- Very large masses: $M_{H_2} \sim 900$ GeV: For M_{H_2} as large as 900 GeV, the signal cross-section after imposing the selection cuts becomes extremely low, $\sigma \sim 0.06$ fb. Here, we thus use higher trigger and selection cuts as is given in Table VI and Table VII, in order to reduce the background.

In order to perform the multivariate analysis, we choose a set of 27 kinematic variables with excellent discriminating power, which are $M_{\ell jj\nu}$, $p_T(\ell)$, $\eta(\ell)$, $p_T(j_i)$, $\eta(j_i)$, \cancel{E}_T , $\phi(\cancel{E}_T)$, $p_T(\ell, \cancel{E}_T)$, $p_T(j_1, j_2)$, $|\Delta\phi(W_1, W_2)|$, $|\Delta\phi(\ell, j_1)|$, $\Delta\eta(\ell, j_2)$, $\Delta\eta(\ell, j_i)$, $|\Delta\phi(j_1, j_2)|$, $\Delta\eta(j_1, j_2)$, $|\Delta\phi(j_i, \cancel{E}_T)|$, S_T , $M_{j_i\ell}$, $M_{j_1j_2\ell}$, $\Delta R(\ell, j_i)$ and $\Delta R(j_1j_2)$. In the above, $i = 1, 2$ and the jets and the reconstructed W s are p_T sorted.

The results for the cut-based and the multivariate analyses are shown in Tables VIII and IX. As expected, we find the MVA to be performing better with respect to the cut-based analysis. Fig. 12 shows the normalised distributions of the signal and background as a function of the BDT response for two benchmark masses, i.e. $M_{H_2} = 350$ GeV

M_{H_2} (GeV)	$\mathcal{N}_{S_{100}}^{BDT}$	$\mathcal{N}_{B_{100}}^{BDT}$	$\mathcal{N}_{S_{3000}}^{BDT}$	$\mathcal{N}_{B_{3000}}^{BDT}$
350	591	116793	17731	3503792
500	309	18761	9270	562838
700	68	3718	2055	111544
900	12	1358	366	40735

TABLE IX. The signal and background events after BDT cut for different Higgs masses. The $\mathcal{N}_{S_{100}/B_{100}}^{BDT}$, $\mathcal{N}_{S_{3000}/B_{3000}}^{BDT}$ are the signal and background events with 100 and 3000 fb^{-1} integrated luminosities.

and 500 GeV. We see that for both cases, there is a large region of overlap between the signal and background. This implies that even with a BDT, the separation of signal and background is challenging, resulting in a very small $S/B \lesssim 1/100$. Assuming zero systematic uncertainties we quote the statistical significance in Table X. The discovery potential of H_2 in this channel is however bleak.

M_{H_2} GeV	\mathcal{L} [fb^{-1}]	n_{CBA}	n_{BDT}
350	100	1.34	1.73
	3000	7.36	9.45
500	100	1.80	2.24
	3000	9.86	12.26
700	100	0.94	1.11
	3000	5.17	6.10
900	100	0.26	0.33
	3000	1.41	1.81

TABLE X. The significance for cut-based and multivariate analysis for integrated luminosity 100 fb^{-1} and 3000 fb^{-1} .

VI. NON-STANDARD HEAVY HIGGS PRODUCTION

In addition to the standard production processes, i.e. gluon fusion, VBF , VH_2 ($V = W, Z$), $t\bar{t}H_2$, the heavy Higgs H_2 can also be produced in association with a Z' [52, 57]

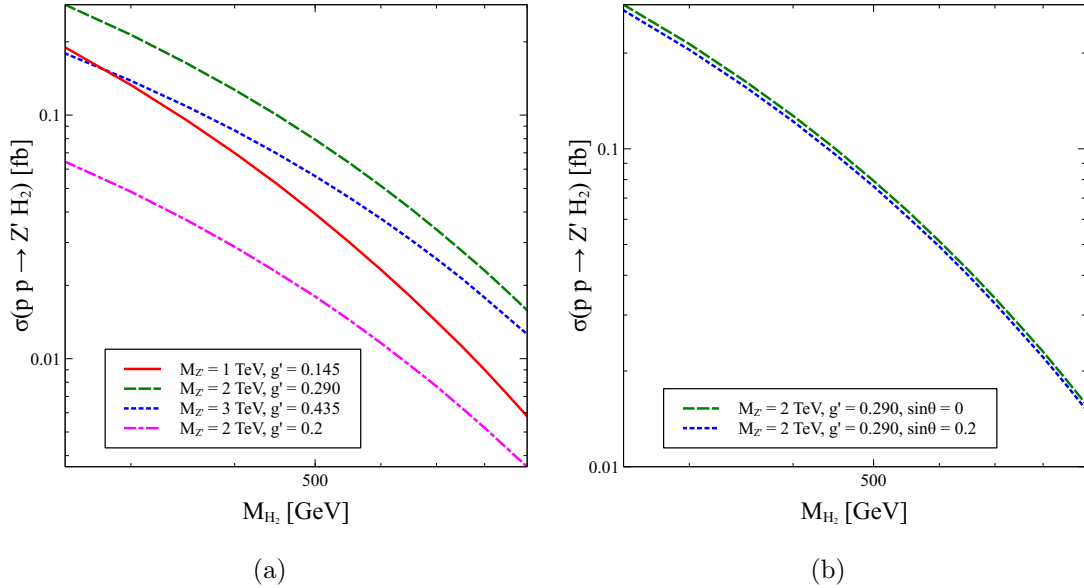


FIG. 13. Left panel: The LO cross-section for the associated production $pp \rightarrow Z'H_2$ for mixing $\theta = 0$ and different values of $M_{Z'}$ and g' (solid red, dashed green, dotted blue and dot-dashed magenta for $[M_{Z'} = 1 \text{ TeV}, g' = 0.145]$, $[M_{Z'} = 2 \text{ TeV}, g' = 0.290]$, $[M_{Z'} = 3 \text{ TeV}, g' = 0.435]$ and $[M_{Z'} = 2 \text{ TeV}, g' = 0.2]$ respectively) such that $\frac{M_{Z'}}{g'} \geq 6.9 \text{ TeV}$ (Eq. 21). Right panel: Comparison between the associated production $pp \rightarrow Z'H_2$ between $\sin\theta = 0$ and $\sin\theta = 0.2$ (dashed green and dotted blue are for $[M_{Z'} = 2 \text{ TeV}, g' = 0.290, \sin\theta = 0]$ and $[M_{Z'} = 2 \text{ TeV}, g' = 0.290, \sin\theta = 0.2]$ respectively).

². In the decoupling limit, the mixing $\theta \sim 0$ and hence the gluon fusion contribution would be negligible. However, the vertex factor $Z'Z'H_2$ is proportional to $\cos\theta$ (see Eq. 17). Therefore, even in the decoupling limit, the process $pp \rightarrow Z'H_2$ will give a non-zero contribution. We show the production cross-section of this process in Fig. 13a for the decoupling limit. Note that, for a non-zero value of θ , both the s -channel ($pp \rightarrow Z'^* \rightarrow H_2Z'$)³ and t -channel diagrams mediated by quarks will contribute (see Fig. 13b). However, the t -channel contribution will be small.

VII. DECAY TO HEAVY NEUTRINOS

Here we briefly discuss the decay of H_2 to two heavy neutrino states, *i.e.*, $pp \rightarrow H_2 \rightarrow N_R N_R$. The unique feature of the $B - L$ model is that both Z' and H_2 can decay to

² For a complete list of production processes, see [51, 57, 58].

³ Note that, $Z'H_2\gamma$ contribution is negligible because the vertex is loop suppressed and also because in the minimal $B - L$ scenario, the $Z'W^+W^-$ coupling is absent. Hence, we neglect this contribution in our study.

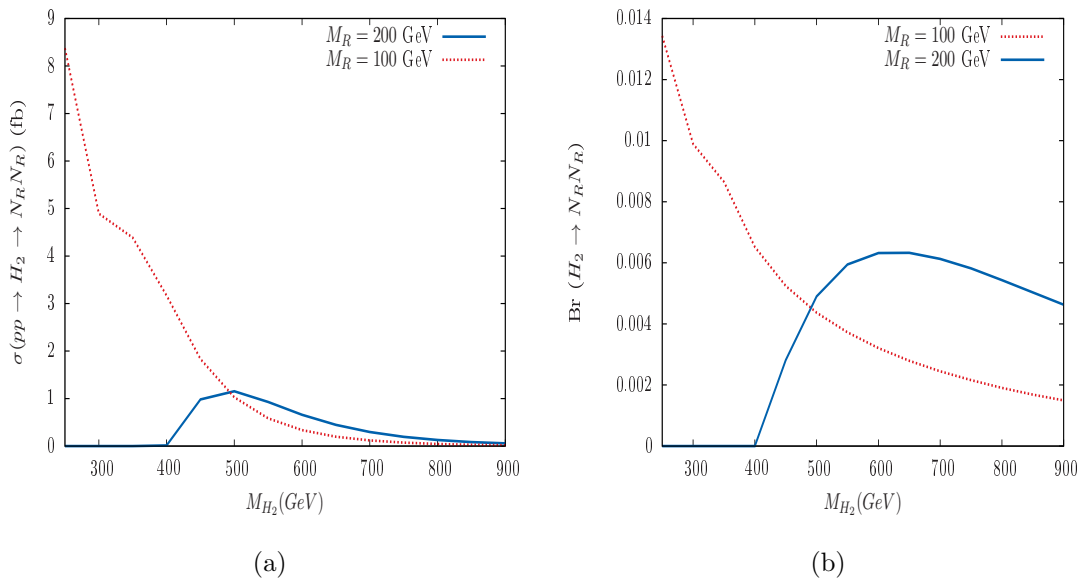


FIG. 14. Left panel: The NNLO production cross-section of $pp \rightarrow H_2 \rightarrow N_R N_R$. Right panel: The branching ratios of $H_2 \rightarrow N_R N_R$ (solid blue : $M_R = 200$ GeV and dotted red : $M_R = 100$ GeV).

a pair of heavy neutrinos. These produced heavy neutrinos can further decay to lW , νZ and $H_1 \nu$ states, producing same as well as opposite sign leptonic signatures. The same sign leptonic signature confirms the Majorana nature of the heavy neutrinos, as well as, the presence of $B - L$ breaking⁴. In Ref. [54] the authors have studied the same sign dilepton+4-jets signature from $pp \rightarrow Z' \rightarrow N_R N_R$ channel. In Ref. [55], multilepton final states have been studied. In Fig. 14a we show the NNLO cross-section of $pp \rightarrow H_2 \rightarrow N_R N_R$, which is only few fb for $M_N = 100$ GeV. In addition, we also show the branching ratio of $H_2 \rightarrow N_R N_R$ in Fig. 14b. Note that, this branching ratio is small. Hence, even for lower N_R masses, e.g. 100 or 200 GeV, the previous analysis of $pp \rightarrow H_2 \rightarrow W^+ W^-$ and $pp \rightarrow H_2 \rightarrow ZZ$ will remain practically unchanged. A detailed study for $pp \rightarrow h_2 \rightarrow N_R N_R$ has been presented in Refs. [57, 58]. This channel also offers other final states, e.g. $l^\pm l^\pm + 4j$, $l^\pm l^\mp l^\pm + 2j + \cancel{E}_T$, $4l + \cancel{E}_T$, $4b + \cancel{E}_T$ and $l + \cancel{E}_T + b\bar{b} + 2j$.

VIII. SUMMARY AND CONCLUSIONS

The gauged $B - L$ model is well-motivated and phenomenologically rich. Three heavy neutrinos, required for anomaly cancellation, participate in the *seesaw* mechanism and

⁴ Same sign dileptonic signature can also arise from a Higgs triplet Type-II seesaw scenario [129]

generate viable light neutrino masses and mixings. In addition to the heavy neutrinos, this model has an extra Z' gauge boson and an additional SM-singlet Higgs state. In this work, we studied in detail the discovery prospect of the gauged $B - L$ model through the Higgs window. We considered the $B - L$ breaking scale to be few TeV, for which the Z' and the heavy neutrinos are naturally of TeV scale, and we considered heavy Higgs masses starting from 250 GeV up to 900 GeV.

The SM-singlet Higgs state mixes with the SM Higgs with a mixing angle θ , that is constrained by direct and indirect searches, such as, vacuum stability, electroweak precision data and M_W mass measurement. The precise determination of the SM Higgs masses and the compatibility of its couplings with the SM prediction bounds the mixing angle to be $\sin^2 \theta \lesssim 0.3$. However, the most stringent limit on the mixing angle arises from the M_W mass measurement. In section IV, we reviewed the different constraints and for our subsequent analysis we consider the mixing angle $\sin \theta = 0.2$, compatible with M_W mass measurement.

During future LHC runs, Higgs coupling measurements can provide strong indirect constraints on the mixing angle between the SM-like Higgs boson and the heavy neutral Higgs, independent of the mass of the heavy state. The predicted bound on $\sin \theta$ from the 14 TeV run of LHC with $\int \mathcal{L} dt = 300 \text{ fb}^{-1}$ is $\sin \theta \sim 0.36$ from the $H \rightarrow WW^*$ coupling measurement. However, if $m_{H_2} \lesssim 500 \text{ GeV}$ direct searches will be more sensitive.

The heavy Higgs of this model can be produced via gluon fusion, VBF, associated Higgs production, out of which the gluon fusion offers the highest cross-section. We considered $pp \rightarrow H_2$ folded with H_2 decaying into different SM states. For our parameters of interest, H_2 does not decay to any additional invisibles state. The produced H_2 decays predominantly to W^+W^- , H_1H_1 and ZZ final states. The decays of the gauge bosons lead to different final states, such as 4ℓ and $lj j \cancel{E}_T$. We studied the discovery prospect of a heavy Higgs H_2 in the 4ℓ , $2\ell 2j$ and the $lj j \cancel{E}_T$ channels at the LHC (with $\int \mathcal{L} dt = 100 \text{ fb}^{-1}$) and HL-LHC ($\int \mathcal{L} dt = 3000 \text{ fb}^{-1}$), where we employed a boosted decision tree to separate signal from background.

The channel with four leptons was found to be the cleanest. The signal and background cross-sections for these processes are $\sigma_S \simeq 0.1 \text{ fb}$ and $\sigma_B \simeq 42 \text{ pb}$, respectively. Using the cuts on the i) invariant mass of 4ℓ and on the reconstructed Z bosons, ii) the p_T cuts on the momenta of four leptons, as well as, the reconstructed Z bosons, we found that for a mass $M_{H_2} \leq 500 \text{ GeV}$, the H_2 can be discovered with a significance of $\sim 5\sigma$ at HL-LHC

with 3000 fb^{-1} .

The $ZZ \rightarrow 2\ell 2j$ final state has a larger cross section than the 4ℓ final state. Particularly for heavy H_2 masses an increased cross section is important to extend the LHC's reach. However, we find that for small mixing angles ($\sin \theta = 0.2$) this channel has small S/B and sensitivity.

$pp \rightarrow H_2 \rightarrow W^+W^- \rightarrow \ell jj \cancel{E}_T$ offers an even larger cross-section for the signal, i.e. $\sigma \simeq \mathcal{O}(10) \text{ fb}$. Unfortunately, huge backgrounds $\sigma_B \simeq \mathcal{O}(10^3) \text{ pb}$ make this channel extremely difficult to deal with. We explored the different mass regions of the heavy Higgs M_{H_2} and applied exclusive trigger and selection cuts. We found that in the most optimistic scenario, assuming zero systematic uncertainties, a heavy Higgs search for $350 \leq M_{H_2} \leq 700 \text{ GeV}$ has a statistical significance of 2.24σ with 100 fb^{-1} and up to 5σ with 3000 fb^{-1} . Since entirely negligible systematic uncertainties are not realistic in this fairly complex final state with jets and missing-transverse energy, even using data-driven methods only, the 4ℓ channel proves to be superior in discovering a heavy Higgs boson in the $B - L$ model.

The heavy Higgs H_2 decays to H_1H_1 with a branching ratio $\sim 20\%$ for $M_{H_2} \gtrsim 400 \text{ GeV}$. Due to the small production cross section for $H_2 \rightarrow H_1H_1 \rightarrow b\bar{b}b\bar{b}$ or $H_2 \rightarrow H_1H_1 \rightarrow b\bar{b}\gamma\gamma$ searching for H_2 in these final states is very challenging. However, we showed that for M_{H_2} up to 500 GeV , the production cross-section for $pp \rightarrow H_1H_1$ is significantly enhanced with respect to the SM expectation. Hence, it might be interesting to look for this channel in this region of the parameter space in more details.

In this analysis, we also briefly considered the Z' searches. We used the ATLAS search at 8 TeV for Z' in the dileptonic channel to recast Z' mass constraints for various values of the $U(1)_{B-L}$ coupling g' and the heavy neutrino masses, M_N .

ACKNOWLEDGEMENTS

S.B. and M.M. would like to thank Satyaki Bhattacharya, Shilpi Jain, Arghya Choudhury, Tanumoy Mandal and Saurabh Niyogi for some helpful discussions regarding `TMVA` and `FastJet`. The work of S.B. was partially supported by funding available from the Department of Atomic Energy, Government of India for the Regional Centre for Accelerator-based Particle Physics (RECAPP), Harish-Chandra Research Institute. S.B. and M.M. would also like to acknowledge the hospitality of IPPP, Durham, where the work began. The work of M.M. was partially supported by DST-Inspire project grant. This research

was supported in part by the European Commission through the 'HiggsTools' Initial Training Network PITN-GA-2012-316704.

- [1] **ATLAS** Collaboration, G. Aad et al., *Observation of a new particle in the search for the Standard Model Higgs boson with the ATLAS detector at the LHC*, *Phys.Lett.* **B716** (2012) 1–29, [[arXiv:1207.7214](#)].
- [2] **CMS** Collaboration, S. Chatrchyan et al., *Observation of a new boson at a mass of 125 GeV with the CMS experiment at the LHC*, *Phys.Lett.* **B716** (2012) 30–61, [[arXiv:1207.7235](#)].
- [3] **ATLAS, CMS** Collaboration, G. Aad et al., *Combined Measurement of the Higgs Boson Mass in pp Collisions at $\sqrt{s} = 7$ and 8 TeV with the ATLAS and CMS Experiments*, [[arXiv:1503.07589](#)].
- [4] E. Massó and V. Sanz, *Limits on anomalous couplings of the Higgs boson to electroweak gauge bosons from LEP and the LHC*, *Phys.Rev.* **D87** (2013), no. 3 033001, [[arXiv:1211.1320](#)].
- [5] T. Corbett, O. Eboli, J. Gonzalez-Fraile, and M. Gonzalez-Garcia, *Robust Determination of the Higgs Couplings: Power to the Data*, *Phys.Rev.* **D87** (2013) 015022, [[arXiv:1211.4580](#)].
- [6] A. Falkowski, F. Riva, and A. Urbano, *Higgs at last*, *JHEP* **1311** (2013) 111, [[arXiv:1303.1812](#)].
- [7] T. Corbett, O. Eboli, J. Gonzalez-Fraile, and M. Gonzalez-Garcia, *Determining Triple Gauge Boson Couplings from Higgs Data*, *Phys.Rev.Lett.* **111** (2013) 011801, [[arXiv:1304.1151](#)].
- [8] B. Dumont, S. Fichet, and G. von Gersdorff, *A Bayesian view of the Higgs sector with higher dimensional operators*, *JHEP* **1307** (2013) 065, [[arXiv:1304.3369](#)].
- [9] S. Banerjee, S. Mukhopadhyay, and B. Mukhopadhyaya, *New Higgs interactions and recent data from the LHC and the Tevatron*, *JHEP* **1210** (2012) 062, [[arXiv:1207.3588](#)].
- [10] J. S. Gainer, J. Lykken, K. T. Matchev, S. Mrenna, and M. Park, *Geolocating the Higgs Boson Candidate at the LHC*, *Phys.Rev.Lett.* **111** (2013) 041801, [[arXiv:1304.4936](#)].
- [11] T. Corbett, O. J. P. Éboli, J. Gonzalez-Fraile, and M. Gonzalez-Garcia, *Robust determination of the scalar boson couplings*, [[arXiv:1306.0006](#)].

- [12] J. Elias-Miro, J. Espinosa, E. Masso, and A. Pomarol, *Higgs windows to new physics through $d=6$ operators: constraints and one-loop anomalous dimensions*, *JHEP* **1311** (2013) 066, [[arXiv:1308.1879](#)].
- [13] A. Pomarol and F. Riva, *Towards the Ultimate SM Fit to Close in on Higgs Physics*, *JHEP* **1401** (2014) 151, [[arXiv:1308.2803](#)].
- [14] M. B. Einhorn and J. Wudka, *Higgs-Boson Couplings Beyond the Standard Model*, *Nucl.Phys.* **B877** (2013) 792–806, [[arXiv:1308.2255](#)].
- [15] S. Banerjee, S. Mukhopadhyay, and B. Mukhopadhyaya, *Higher dimensional operators and the LHC Higgs data: The role of modified kinematics*, *Phys.Rev.* **D89** (2014), no. 5 053010, [[arXiv:1308.4860](#)].
- [16] S. Willenbrock and C. Zhang, *Effective Field Theory Beyond the Standard Model*, *Ann.Rev.Nucl.Part.Sci.* **64** (2014) 83–100, [[arXiv:1401.0470](#)].
- [17] J. Ellis, V. Sanz, and T. You, *Complete Higgs Sector Constraints on Dimension-6 Operators*, *JHEP* **1407** (2014) 036, [[arXiv:1404.3667](#)].
- [18] H. Belusca-Maito, *Effective Higgs Lagrangian and Constraints on Higgs Couplings*, [[arXiv:1404.5343](#)].
- [19] R. S. Gupta, A. Pomarol, and F. Riva, *BSM Primary Effects*, *Phys.Rev.* **D91** (2015), no. 3 035001, [[arXiv:1405.0181](#)].
- [20] E. Masso, *An Effective Guide to Beyond the Standard Model Physics*, *JHEP* **1410** (2014) 128, [[arXiv:1406.6376](#)].
- [21] A. Biekter, A. Knochel, M. Krmer, D. Liu, and F. Riva, *Vices and virtues of Higgs effective field theories at large energy*, *Phys.Rev.* **D91** (2015) 055029, [[arXiv:1406.7320](#)].
- [22] C. Englert and M. Spannowsky, *Effective Theories and Measurements at Colliders*, *Phys.Lett.* **B740** (2015) 8–15, [[arXiv:1408.5147](#)].
- [23] J. Ellis, V. Sanz, and T. You, *The Effective Standard Model after LHC Run I*, *JHEP* **1503** (2015) 157, [[arXiv:1410.7703](#)].
- [24] R. Edezhath, *Dimension-6 Operator Constraints from Boosted VBF Higgs*, [[arXiv:1501.00992](#)].
- [25] M. Gorbahn, J. M. No, and V. Sanz, *Benchmarks for Higgs Effective Theory: Extended Higgs Sectors*, [[arXiv:1502.07352](#)].
- [26] Z. Han and W. Skiba, *Effective theory analysis of precision electroweak data*, *Phys.Rev.* **D71** (2005) 075009, [[hep-ph/0412166](#)].

- [27] M. Ciuchini, E. Franco, S. Mishima, and L. Silvestrini, *Electroweak Precision Observables, New Physics and the Nature of a 126 GeV Higgs Boson*, *JHEP* **1308** (2013) 106, [[arXiv:1306.4644](#)].
- [28] J. de Blas, *Electroweak limits on physics beyond the Standard Model*, *EPJ Web Conf.* **60** (2013) 19008, [[arXiv:1307.6173](#)].
- [29] C.-Y. Chen, S. Dawson, and C. Zhang, *Electroweak Effective Operators and Higgs Physics*, *Phys.Rev.* **D89** (2014), no. 1 015016, [[arXiv:1311.3107](#)].
- [30] R. Alonso, E. E. Jenkins, A. V. Manohar, and M. Trott, *Renormalization Group Evolution of the Standard Model Dimension Six Operators III: Gauge Coupling Dependence and Phenomenology*, *JHEP* **1404** (2014) 159, [[arXiv:1312.2014](#)].
- [31] C. Englert, A. Freitas, M. Hlileitner, T. Plehn, M. Rauch, et al., *Precision Measurements of Higgs Couplings: Implications for New Physics Scales*, *J.Phys.* **G41** (2014) 113001, [[arXiv:1403.7191](#)].
- [32] M. Trott, *On the consistent use of Constructed Observables*, *JHEP* **1502** (2015) 046, [[arXiv:1409.7605](#)].
- [33] A. Falkowski and F. Riva, *Model-independent precision constraints on dimension-6 operators*, *JHEP* **1502** (2015) 039, [[arXiv:1411.0669](#)].
- [34] B. Henning, X. Lu, and H. Murayama, *How to use the Standard Model effective field theory*, [[arXiv:1412.1837](#)].
- [35] J. de Blas, M. Chala, M. Perez-Victoria, and J. Santiago, *Observable Effects of General New Scalar Particles*, [[arXiv:1412.8480](#)].
- [36] L. Berthier and M. Trott, *Towards consistent Electroweak Precision Data constraints in the SMEFT*, [[arXiv:1502.02570](#)].
- [37] A. Efrati, A. Falkowski, and Y. Soreq, *Electroweak constraints on flavorful effective theories*, [[arXiv:1503.07872](#)].
- [38] E. D. Carlson, *Limits On A New U(1) Coupling*, *Nucl. Phys. B* **286**, 378 (1987).
- [39] R. N. Mohapatra and J. C. Pati, *Left-Right Gauge Symmetry and an Isoconjugate Model of CP Violation*, *Phys.Rev.* **D11** (1975) 566–571.
- [40] R. Mohapatra and J. C. Pati, *A Natural Left-Right Symmetry*, *Phys.Rev.* **D11** (1975) 2558.
- [41] G. Senjanovic and R. N. Mohapatra, *Exact Left-Right Symmetry and Spontaneous Violation of Parity*, *Phys.Rev.* **D12** (1975) 1502.

- [42] P.-H. Gu, *Mirror left-right symmetry*, *Phys.Lett.* **B713** (2012) 485–489, [[arXiv:1201.3551](#)].
- [43] **CMS Collaboration** Collaboration, V. Khachatryan et al., *Search for heavy neutrinos and W bosons with right-handed couplings in proton-proton collisions at $\sqrt{s} = 8$ TeV*, *Eur.Phys.J.* **C74** (2014), no. 11 3149, [[arXiv:1407.3683](#)].
- [44] W. Buchmuller, C. Greub, and P. Minkowski, *Neutrino masses, neutral vector bosons and the scale of B-L breaking*, *Phys.Lett.* **B267** (1991) 395–399.
- [45] P. Minkowski, $\mu \rightarrow e\gamma$ at a Rate of One Out of 10^9 Muon Decays?, *Phys.Lett.* **B67** (1977) 421–428.
- [46] R. N. Mohapatra and G. Senjanovic, *Neutrino Mass and Spontaneous Parity Violation*, *Phys.Rev.Lett.* **44** (1980) 912.
- [47] T. Yanagida, *Horizontal Symmetry and Masses of Neutrinos*, *Prog.Theor.Phys.* **64** (1980) 1103.
- [48] J. Schechter and J. Valle, *Neutrino Masses in $SU(2) \times U(1)$ Theories*, *Phys.Rev.* **D22** (1980) 2227.
- [49] M. Fukugita and T. Yanagida, *Baryogenesis Without Grand Unification*, *Phys.Lett.* **B174** (1986) 45.
- [50] J. Gluza, *On teraelectronvolt Majorana neutrinos*, *Acta Phys.Polon.* **B33** (2002) 1735–1746, [[hep-ph/0201002](#)].
- [51] W. Emam and S. Khalil, *Higgs and Z-prime phenomenology in B-L extension of the standard model at LHC*, *Eur.Phys.J.* **C52** (2007) 625–633, [[arXiv:0704.1395](#)].
- [52] L. Basso, A. Belyaev, S. Moretti, and C. H. Shepherd-Themistocleous, *Phenomenology of the minimal B-L extension of the Standard model: Z' and neutrinos*, *Phys.Rev.* **D80** (2009) 055030, [[arXiv:0812.4313](#)].
- [53] L. Basso, A. Belyaev, S. Moretti, and G. M. Pruna, *Probing the Z-prime sector of the minimal B-L model at future Linear Colliders in the $e^+e^- \rightarrow \mu^+\mu^-$ process*, *JHEP* **0910** (2009) 006, [[arXiv:0903.4777](#)].
- [54] P. Fileviez Perez, T. Han, and T. Li, *Testability of Type I Seesaw at the CERN LHC: Revealing the Existence of the B-L Symmetry*, *Phys.Rev.* **D80** (2009) 073015, [[arXiv:0907.4186](#)].
- [55] K. Huitu, S. Khalil, H. Okada and S. K. Rai, *Signatures for right-handed neutrinos at the Large Hadron Collider*, *Phys. Rev. Lett.* **101**, 181802 (2008), [[arXiv:0803.2799](#)].

- [56] L. Basso, S. Moretti, and G. M. Pruna, *The Higgs sector of the minimal $B - L$ model at future Linear Colliders*, *Eur.Phys.J.* **C71** (2011) 1724, [[arXiv:1012.0167](#)].
- [57] G. M. Pruna, *Phenomenology of the minimal $B - L$ Model: the Higgs sector at the Large Hadron Collider and future Linear Colliders*, [[arXiv:1106.4691](#)].
- [58] L. Basso, S. Moretti and G. M. Pruna, *Phenomenology of the minimal $B - L$ extension of the Standard Model: the Higgs sector*, *Phys. Rev. D* **83**, 055014 (2011) [[arXiv:1011.2612](#)].
- [59] C. Englert, T. Plehn, D. Zerwas, and P. M. Zerwas, *Exploring the Higgs portal*, *Phys.Lett.* **B703** (2011) 298–305, [[arXiv:1106.3097](#)].
- [60] V. V. Khoze and G. Ro, *Leptogenesis and Neutrino Oscillations in the Classically Conformal Standard Model with the Higgs Portal*, *JHEP* **1310** (2013) 075, [[arXiv:1307.3764](#)].
- [61] J. Hernández López and J. Orduz-Ducucara, *A calculation for $Br(Z' \rightarrow tth)$ in a $B-L$ model*, *J.Phys.Conf.Ser.* **468** (2013) 012012.
- [62] L. Basso, *Minimal Z' models and the 125 GeV Higgs boson*, *Phys.Lett.* **B725** (2013) 322–326, [[arXiv:1303.1084](#)].
- [63] J. Gluza and T. Jelinski, *Heavy neutrinos and the $pp \rightarrow lljj$ CMS data*, [[arXiv:1504.05568](#)].
- [64] W.-Y. Keung and G. Senjanovic, *Majorana Neutrinos and the Production of the Right-handed Charged Gauge Boson*, *Phys.Rev.Lett.* **50** (1983) 1427.
- [65] **CMS Collaboration** Collaboration, *Search for Heavy Resonances Decaying into bb and bg Final States in pp Collisions at $\sqrt{s} = 8$ TeV*, .
- [66] **ATLAS Collaboration**, G. Aad et al., *Search for high-mass dilepton resonances in pp collisions at $\sqrt{s} = 8$ TeV with the ATLAS detector*, *Phys.Rev.* **D90** (2014), no. 5 052005, [[arXiv:1405.4123](#)].
- [67] **CMS Collaboration**, V. Khachatryan et al., *Search for physics beyond the standard model in dilepton mass spectra in proton-proton collisions at $\sqrt{s} = 8$ TeV*, *JHEP* **1504** (2015) 025, [[arXiv:1412.6302](#)].
- [68] **CMS Collaboration**, V. Khachatryan et al., *Search for resonances and quantum black holes using dijet mass spectra in proton-proton collisions at $\sqrt{s} = 8$ TeV*, *Phys.Rev.* **D91** (2015), no. 5 052009, [[arXiv:1501.04198](#)].
- [69] **CMS Collaboration**, S. Chatrchyan et al., *Search for Anomalous $t\bar{t}$ Production in the Highly-Boosted All-Hadronic Final State*, *JHEP* **1209** (2012) 029, [[arXiv:1204.2488](#)].

- [70] **ATLAS** Collaboration, G. Aad et al., *A search for high-mass resonances decaying to $\tau^+\tau^-$ in pp collisions at $\sqrt{s} = 8$ TeV with the ATLAS detector*, [[arXiv:1502.07177](#)].
- [71] T. Robens and T. Stefaniak, *Status of the Higgs Singlet Extension of the Standard Model after LHC Run 1*, *Eur.Phys.J.* **C75** (2015), no. 3 104, [[arXiv:1501.02234](#)].
- [72] D. Lopez-Val and T. Robens, *r and the W-boson mass in the singlet extension of the standard model*, *Phys.Rev.* **D90** (2014), no. 11 114018, [[arXiv:1406.1043](#)].
- [73] **ALEPH, DELPHI, L3, OPAL, LEP Electroweak Working Group** Collaboration, J. Alcaraz et al., *A Combination of preliminary electroweak measurements and constraints on the standard model*, [[hep-ex/0612034](#)].
- [74] **CMS** Collaboration, V. Khachatryan et al., *Precise determination of the mass of the Higgs boson and tests of compatibility of its couplings with the standard model predictions using proton collisions at 7 and 8 TeV*, *Eur.Phys.J.* **C75** (2015), no. 5 212, [[arXiv:1412.8662](#)].
- [75] **ATLAS** Collaboration, *Measurements of the Higgs boson production and decay rates and coupling strengths using pp collision data at $s = 7$ and 8 TeV in the ATLAS experiment*, [[ATLAS-CONF-2015-007](#)].
- [76] D. Feldman, P. Fileviez Perez and P. Nath, *R-parity Conservation via the Stueckelberg Mechanism: LHC and Dark Matter Signals*, *JHEP* **1201**, 038 (2012), [[arXiv:1109.2901](#)].
- [77] J. Heeck, *Unbroken B-L Symmetry*, *Phys.Lett.* **B739** (2014) 256–262, [[arXiv:1408.6845](#)].
- [78] P. Fileviez Perez, S. Spinner and M. K. Trenkel, *The LSP Stability and New Higgs Signals at the LHC*, *Phys. Rev. D* **84**, 095028 (2011), [[arXiv:1103.5504](#)].
- [79] B. Kors and P. Nath, *A Stueckelberg extension of the standard model*, *Phys. Lett. B* **586**, 366 (2004), [[hep-ph/0402047](#)].
- [80] B. Kors and P. Nath, *Aspects of the Stueckelberg extension*, *JHEP* **0507**, 069 (2005) [[hep-ph/0503208](#)].
- [81] R. Marshak and R. N. Mohapatra, *Quark - Lepton Symmetry and B-L as the U(1) Generator of the Electroweak Symmetry Group*, *Phys.Lett.* **B91** (1980) 222–224.
- [82] R. N. Mohapatra and R. Marshak, *Local B-L Symmetry of Electroweak Interactions, Majorana Neutrinos and Neutron Oscillations*, *Phys.Rev.Lett.* **44** (1980) 1316–1319.
- [83] C. Wetterich, *Neutrino Masses and the Scale of B-L Violation*, *Nucl.Phys.* **B187** (1981) 343.

- [84] A. Masiero, J. Nieves, and T. Yanagida, *$B^{-}l$ Violating Proton Decay and Late Cosmological Baryon Production*, *Phys.Lett.* **B116** (1982) 11.
- [85] R. N. Mohapatra and G. Senjanovic, *Spontaneous Breaking of Global $B^{-}l$ Symmetry and Matter - Antimatter Oscillations in Grand Unified Theories*, *Phys.Rev.* **D27** (1983) 254.
- [86] A. Djouadi, *The Anatomy of electro-weak symmetry breaking. I: The Higgs boson in the standard model*, *Phys.Rept.* **457** (2008) 1–216, [[hep-ph/0503172](#)].
- [87] A. Atre, T. Han, S. Pascoli, and B. Zhang, *The Search for Heavy Majorana Neutrinos*, *JHEP* **0905** (2009) 030, [[arXiv:0901.3589](#)].
- [88] M. Mitra, G. Senjanovic, and F. Vissani, *Neutrinoless Double Beta Decay and Heavy Sterile Neutrinos*, *Nucl.Phys.* **B856** (2012) 26–73, [[arXiv:1108.0004](#)].
- [89] F. F. Deppisch, P. S. B. Dev, and A. Pilaftsis, *Neutrinos and Collider Physics*, [[arXiv:1502.06541](#)].
- [90] M. Carena, A. Daleo, B. A. Dobrescu, and T. M. Tait, *Z' gauge bosons at the Tevatron*, *Phys.Rev.* **D70** (2004) 093009, [[hep-ph/0408098](#)].
- [91] G. Cacciapaglia, C. Csaki, G. Marandella, and A. Strumia, *The Minimal Set of Electroweak Precision Parameters*, *Phys.Rev.* **D74** (2006) 033011, [[hep-ph/0604111](#)].
- [92] **ATLAS** Collaboration, G. Aad et al., *Search for resonances decaying into top-quark pairs using fully hadronic decays in pp collisions with ATLAS at $\sqrt{s} = 7$ TeV*, *JHEP* **1301** (2013) 116, [[arXiv:1211.2202](#)].
- [93] T. Mandal, S. Mitra, and S. Seth, *Single Productions of Colored Particles at the LHC: An Example with Scalar Leptoquarks*, [[arXiv:1503.04689](#)].
- [94] **LHC Higgs Cross Section Working Group** Collaboration, S. Heinemeyer et al., *Handbook of LHC Higgs Cross Sections: 3. Higgs Properties*, [[arXiv:1307.1347](#)].
- [95] M. E. Peskin, *Comparison of LHC and ILC Capabilities for Higgs Boson Coupling Measurements*, [[arXiv:1207.2516](#)].
- [96] **CDF** Collaboration, T. Aaltonen et al., *Precise measurement of the W -boson mass with the CDF II detector*, *Phys.Rev.Lett.* **108** (2012) 151803, [[arXiv:1203.0275](#)].
- [97] **D0** Collaboration, V. M. Abazov et al., *Measurement of the W boson mass with the D0 detector*, *Phys.Rev.* **D89** (2014), no. 1 012005, [[arXiv:1310.8628](#)].
- [98] V. Martin-Lozano, J. M. Moreno, and C. B. Park, *Resonant Higgs boson pair production in the $hh \rightarrow b\bar{b} WW \rightarrow b\bar{b}\ell^+\nu\ell^-\bar{\nu}$ decay channel*, [[arXiv:1501.03799](#)].

- [99] G. Altarelli and R. Barbieri, *Vacuum polarization effects of new physics on electroweak processes*, *Phys.Lett.* **B253** (1991) 161–167.
- [100] M. E. Peskin and T. Takeuchi, *A New constraint on a strongly interacting Higgs sector*, *Phys.Rev.Lett.* **65** (1990) 964–967.
- [101] M. E. Peskin and T. Takeuchi, *Estimation of oblique electroweak corrections*, *Phys.Rev.* **D46** (1992) 381–409.
- [102] I. Maksymyk, C. Burgess, and D. London, *Beyond S, T and U*, *Phys.Rev.* **D50** (1994) 529–535, [[hep-ph/9306267](#)].
- [103] B. W. Lee, C. Quigg, and H. Thacker, *Weak Interactions at Very High-Energies: The Role of the Higgs Boson Mass*, *Phys.Rev.* **D16** (1977) 1519.
- [104] G. M. Pruna and T. Robens, *Higgs singlet extension parameter space in the light of the LHC discovery*, *Phys.Rev.* **D88** (2013), no. 11 115012, [[arXiv:1303.1150](#)].
- [105] R. N. Lerner and J. McDonald, *Gauge singlet scalar as inflaton and thermal relic dark matter*, *Phys.Rev.* **D80** (2009) 123507, [[arXiv:0909.0520](#)].
- [106] A. Alloul, N. D. Christensen, C. Degrande, C. Duhr, and B. Fuks, *FeynRules 2.0 - A complete toolbox for tree-level phenomenology*, *Comput.Phys.Commun.* **185** (2014) 2250–2300, [[arXiv:1310.1921](#)].
- [107] C. Degrande, C. Duhr, B. Fuks, D. Grellscheid, O. Mattelaer, et al., *UFO - The Universal FeynRules Output*, *Comput.Phys.Commun.* **183** (2012) 1201–1214, [[arXiv:1108.2040](#)].
- [108] J. Alwall, R. Frederix, S. Frixione, V. Hirschi, F. Maltoni, et al., *The automated computation of tree-level and next-to-leading order differential cross sections, and their matching to parton shower simulations*, *JHEP* **1407** (2014) 079, [[arXiv:1405.0301](#)].
- [109] T. Sjostrand, S. Mrenna, and P. Z. Skands, *PYTHIA 6.4 Physics and Manual*, *JHEP* **0605** (2006) 026, [[hep-ph/0603175](#)].
- [110] M. Cacciari, G. P. Salam, and G. Soyez, *FastJet User Manual*, *Eur.Phys.J.* **C72** (2012) 1896, [[arXiv:1111.6097](#)].
- [111] M. J. Dolan, C. Englert, and M. Spannowsky, *New Physics in LHC Higgs boson pair production*, *Phys.Rev.* **D87** (2013), no. 5 055002, [[arXiv:1210.8166](#)].
- [112] J. M. No and M. Ramsey-Musolf, *Probing the Higgs Portal at the LHC Through Resonant di-Higgs Production*, *Phys.Rev.* **D89** (2014), no. 9 095031, [[arXiv:1310.6035](#)].
- [113] A. Falkowski, C. Gross, and O. Lebedev, *A second Higgs from the Higgs portal*, *JHEP* **1505** (2015) 057, [[arXiv:1502.01361](#)].

- [114] D. Buttazzo, F. Sala, and A. Tesi, *Singlet-like Higgs bosons at present and future colliders*, [[arXiv:1505.05488](https://arxiv.org/abs/1505.05488)].
- [115] **CMS Collaboration** Collaboration, *Search for resonant HH production in 2gamma+2b channel*, .
- [116] **ATLAS Collaboration**, G. Aad et al., *Search For Higgs Boson Pair Production in the $\gamma\gamma b\bar{b}$ Final State using pp Collision Data at $\sqrt{s} = 8$ TeV from the ATLAS Detector*, *Phys.Rev.Lett.* **114** (2015), no. 8 081802, [[arXiv:1406.5053](https://arxiv.org/abs/1406.5053)].
- [117] **ATLAS Collaboration**, G. Aad et al., *Search for Higgs boson pair production in the $b\bar{b}b\bar{b}$ final state from pp collisions at $\sqrt{s} = 8$ TeV with the ATLAS detector*, [[arXiv:1506.00285](https://arxiv.org/abs/1506.00285)].
- [118] R. Frederix, S. Frixione, V. Hirschi, F. Maltoni, O. Mattelaer, et al., *Higgs pair production at the LHC with NLO and parton-shower effects*, *Phys.Lett.* **B732** (2014) 142–149, [[arXiv:1401.7340](https://arxiv.org/abs/1401.7340)].
- [119] A. Hoecker, P. Speckmayer, J. Stelzer, J. Therhaag, E. von Toerne, H. Voss, M. Backes, T. Carli, O. Cohen, A. Christov, D. Dannheim, K. Danielowski, S. Henrot-Versille, M. Jachowski, K. Kraszewski, A. Krasznahorkay, Jr., M. Kruk, Y. Mahalalel, R. Ospanov, X. Prudent, A. Robert, D. Schouten, F. Tegenfeldt, A. Voigt, K. Voss, M. Wolter, and A. Zemla, *TMVA - Toolkit for Multivariate Data Analysis*, *ArXiv Physics e-prints* (Mar., 2007) [[physics/0703039](https://arxiv.org/abs/physics/0703039)].
- [120] D. Ciupke, “Study of BDT Training Configurations with an Application to the $Z/H \rightarrow \tau\tau \rightarrow ee$ Analysis.” http://www.desy.de/f/students/2012/reports/david_ciupke.pdf.gz, 2012.
- [121] T. Junk, *Confidence level computation for combining searches with small statistics*, *Nucl.Instrum.Meth.* **A434** (1999) 435–443, [[hep-ex/9902006](https://arxiv.org/abs/hep-ex/9902006)].
- [122] C. Hackstein and M. Spannowsky, *Boosting Higgs discovery: The Forgotten channel*, *Phys.Rev.* **D82** (2010) 113012, [[arXiv:1008.2202](https://arxiv.org/abs/1008.2202)].
- [123] J. M. Butterworth, A. R. Davison, M. Rubin, and G. P. Salam, *Jet substructure as a new Higgs search channel at the LHC*, *Phys.Rev.Lett.* **100** (2008) 242001, [[arXiv:0802.2470](https://arxiv.org/abs/0802.2470)].
- [124] S. D. Ellis, C. K. Vermilion, and J. R. Walsh, *Recombination Algorithms and Jet Substructure: Pruning as a Tool for Heavy Particle Searches*, *Phys.Rev.* **D81** (2010) 094023, [[arXiv:0912.0033](https://arxiv.org/abs/0912.0033)].
- [125] S. D. Ellis, C. K. Vermilion, and J. R. Walsh, *Techniques for improved heavy particle searches with jet substructure*, *Phys.Rev.* **D80** (2009) 051501, [[arXiv:0903.5081](https://arxiv.org/abs/0903.5081)].

- [126] D. Krohn, J. Thaler, and L.-T. Wang, *Jet Trimming*, *JHEP* **1002** (2010) 084, [[arXiv:0912.1342](#)].
- [127] D. E. Soper and M. Spannowsky, *Combining subjet algorithms to enhance ZH detection at the LHC*, *JHEP* **1008** (2010) 029, [[arXiv:1005.0417](#)].
- [128] **ATLAS** Collaboration, G. Aad et al., *Search for production of WW/WZ resonances decaying to a lepton, neutrino and jets in pp collisions at $\sqrt{s} = 8$ TeV with the ATLAS detector*, *Eur.Phys.J.* **C75** (2015), no. 5 209, [[arXiv:1503.04677](#)].
- [129] P. Fileviez Perez, T. Han, G. y. Huang, T. Li and K. Wang, *Neutrino Masses and the CERN LHC: Testing Type II Seesaw*, *Phys. Rev. D* **78**, 015018 (2008) [[arXiv:0805.3536](#)].